N 62 54587 FILE COPY NO. 1

NACA TN 2587

NATIONAL ADVISORY COMMITTEE FOR AERONAUTICS

TECHNICAL NOTE 2587

INFLUENCE OF WING AND FUSELAGE ON THE VERTICAL-TAIL CONTRIBUTION TO THE LOW-SPEED ROLLING DERIVATIVES OF MIDWING AIRPLANE MODELS WITH 45° SWEPTBACK SURFACES

By Walter D. Wolhart

Langley Aeronautical Laboratory
Langley Field, Va.

Washington
December 1951

THIS DOCUMENT ON LOAN FROM THE FILES OF
NATIONAL ADVISORY COMMITTEE FOR AERONAUTICS
LANGLEY AERONAUTICAL LABORATORY
LANGLEY FIELD, HAMPTON, VIRGINIA
RETURN TO THE ABOVE ADDRESS.
REQUESTS FOR PUBLICATIONS SHOULD BE ADDRESSED AS FOLLOWS:
NATIONAL ADVISORY COMMITTEE FOR AERONAUTICS
1724 F STREET, N.W.,
WASHINGTON 25, D.C.

1B

NATIONAL ADVISORY COMMITTEE FOR AERONAUTICS

TECHNICAL NOTE 2587

INFLUENCE OF WING AND FUSELAGE ON THE VERTICAL-TAIL CONTRIBUTION TO THE LOW-SPEED ROLLING DERIVATIVES OF MIDWING AIRPLANE MODELS WITH 45° SWEPTBACK SURFACES

By Walter D. Wolhart

SUMMARY

An investigation was made to determine the influence of the wing and fuselage on the vertical-tail contribution to the low-speed rolling derivatives of midwing airplane models with 45° sweptback surfaces.

The results show that the vertical-tail contribution to the rolling derivatives of midwing or near-midwing configurations can be calculated with good accuracy throughout the angle-of-attack range by using available procedures when corrections have been made for the effects of fuselage and wing sidewash at the tail due to roll.

The mutual wing-fuselage interference increments of the wing-fuselage configurations investigated showed no consistent effect of fuselage length. The increments were usually rather small and did not vary appreciably with angle of attack except that the increment in yawing moment due to rolling became quite large at angles of attack above 16°.

The contribution of the fuselage alone to the rolling derivatives was small in comparison with the effects of angle of attack for the other components of the models investigated.

INTRODUCTION

Recent advances in the understanding of the principles of high-speed flight have led to significant changes in the design of the principal components of airplanes such as the incorporation of large amounts of sweep of the wing and tail surfaces. Although the effects of changes in wing design on the stability characteristics have been extensively investigated, there is little information available on the influence of changes in the other components of the airplane. In order to provide such information, the Langley stability tunnel is conducting a series of investigations

with a model having various interchangeable components. The effects on the low-speed static lateral stability characteristics of variations in horizontal-tail size and location, and of vertical-tail size and length and of fuselage shape and length are presented in references 1 and 2, respectively. The effects of variations in vertical-tail size and length and of fuselage length on the yawing stability characteristics are presented in reference 3.

As part of this general investigation, the influence of the wing and fuselage on the vertical-tail contribution to rolling derivatives has been determined by the method of interference increments (reference 4), and the results are presented herein. These results are used to check the validity of present methods of estimating the vertical-tail contribution to the rolling derivatives as well as to derive an empirical relation for estimating the fuselage sidewash due to roll.

SYMBOLS

The data presented herein are in the form of standard NACA coefficients of forces and moments which are referred to the stability system of axes with the origin at the quarter-chord point of the wing mean aerodynamic chord. The positive directions of forces, moments, and angular displacements are shown in figure 1. The coefficients and symbols are defined as follows:

C_L lift coefficient $\left(\frac{L}{qS_W}\right)$

C_D drag coefficient $\left(\frac{D}{qS_W}\right)$

C_Y lateral-force coefficient $\left(\frac{Y}{qS_W}\right)$

C_l rolling-moment coefficient $\left(\frac{L'}{qS_W b_W}\right)$

C_m pitching-moment coefficient $\left(\frac{M}{qS_W \bar{c}_W}\right)$

C_n yawing-moment coefficient $\left(\frac{N}{qS_W b_W}\right)$

L	lift, pounds
D	drag, pounds
Y	lateral force, pounds
L'	rolling moment, foot-pounds
M	pitching moment, foot-pounds
N	yawing moment, foot-pounds
q	dynamic pressure, pounds per square foot $\left(\frac{1}{2}\rho V^2\right)$
V	free-stream velocity, feet per second
ρ	mass density of air, slugs per cubic foot
A	aspect ratio $\left(\frac{b^2}{S}\right)$
b	span, measured perpendicular to fuselage center line, feet
S	area, square feet
c	chord, measured parallel to plane of symmetry, feet
c_r	root chord, feet
c_t	tip chord, feet
$\bar{c}$	mean aerodynamic chord, feet $\left(\text{for example, } \bar{c}_W = \frac{2}{S_W}\int_0^{b_W/2} c_W^2\, dy\right)$
l	fuselage length, feet
l_V	tail length, distance from mounting point to $\bar{c}_V/4$, feet
t	maximum thickness of fuselage, feet
x	chordwise distance from leading edge of root chord to quarter-chord point of any chord, feet

$\bar{x}$ chordwise distance from leading edge of root chord to quarter-chord point of mean aerodynamic chord, feet $\left(\text{for example, } \bar{x}_W = \frac{2}{S_W}\int_0^{b_W/2} c_W x_W \, dy\right)$

y spanwise distance measured from the plane of symmetry, feet

z_V perpendicular distance from fuselage center line to $\bar{c}_V/4$, feet

h perpendicular distance from $\bar{c}_V/4$ of vertical tail to axis of rotation, feet

$\Delta h = z_V - h$

λ taper ratio (c_t/c_r)

Λ angle of sweepback of quarter-chord line, degrees

ψ angle of yaw, degrees

α angle of attack, degrees

σ_1 wing sidewash angle, component of angularity of flow at the vertical tail resulting from interference effect of the rolling wing, positive for positive side force, radians

σ_2 fuselage sidewash angle, component of angularity of flow at the vertical tail resulting from interference effect of the rolling fuselage, positive for positive side force, radians

p rolling angular velocity, radians per second

$\frac{pb}{2V}$ wing-tip helix angle, radians

$\left(C_{L_\alpha}\right)_V$ lift-curve slope of vertical tail (C_L of vertical tail based on vertical-tail area), degrees

$C_{Y_p} = \frac{\partial C_Y}{\partial \frac{pb}{2V}}$

$$C_{n_p} = \frac{\partial C_n}{\partial \frac{pb}{2V}}$$

$$C_{l_p} = \frac{\partial C_l}{\partial \frac{pb}{2V}}$$

$\frac{\partial \sigma_1}{\partial \frac{pb}{2V}}$ rate of change of wing sidewash angle at vertical tail with wing-tip helix angle

$\frac{\partial \sigma_2}{\partial \frac{pb}{2V}}$ rate of change of fuselage sidewash angle at vertical tail with wing-tip helix angle

Subscripts and abbreviations:

W wing

V vertical tail; used with subscripts 1 to 5 to denote the various vertical tails (see fig. 2)

F fuselage; used with subscripts 1 to 3 to denote the various fuselages (see fig. 3)

APPARATUS AND TESTS

The tests of the present investigation were made in the 6-foot-diameter rolling-flow test section of the Langley stability tunnel. This section is equipped with a motor-driven rotor which imparts a twist to the air stream so that a model mounted rigidly in the tunnel is in a field of flow similar to that which exists about an airplane in rolling flight (reference 5). Forces and moments on the model were obtained with the model mounted on a single strut support which was in turn connected to a conventional six-component balance system.

All components of the model used in this investigation were constructed of mahogany. Sketches of the components of the models are presented as figures 2, 3, and 4. The various vertical tails and fuselages are referred to hereinafter by the symbol and number assigned to them in figures 2 and 3. All vertical tails had 45° sweepback of the quarter-chord

line, taper ratio of 0.6, and NACA 65A008 profiles in planes parallel to the fuselage center line. The ratios of tail area to wing area were chosen to cover a range representative of that used for current high-speed airplane configurations. The tails were mounted so that the root chord coincided with the fuselage center line and the tail length was always a constant percent of the fuselage length $\left(\frac{l_V}{l} = 0.42\right)$. The three fuselages (fineness ratios of 5.00, 6.67, and 10.00), having circular-arc profiles and circular cross sections, are shown in figure 3. The coordinates of the fuselages are given in table I.

The wing had an aspect ratio of 4.0, taper ratio of 0.6, sweepback of 45° of the quarter-chord line, and NACA 65A008 profiles parallel to the plane of symmetry. The wing was mounted on the fuselage so that the quarter-chord point of the wing mean aerodynamic chord coincided with the fuselage mounting point (fig. 4). A summary of the geometric characteristics of the various model parts is given in table II. A photograph of one of the model configurations is presented as figure 5.

All the tests were made at a dynamic pressure of 39.7 pounds per square foot, which corresponds to a Mach number of 0.166 and a Reynolds number of 0.891×10^6 based on the wing mean aerodynamic chord. The lift, drag, and pitching-moment characteristics were obtained from tests in straight flow for an angle-of-attack range from about -4° to 28° at 0° angle of yaw. The rolling derivatives were obtained from tests in rolling flow at values of $pb/2V$ of ±0.188, ±0.375, and ±0.563.

CORRECTIONS

Approximate corrections, based on unswept-wing theory, for the effects of jet boundaries have been applied to the angle of attack, the drag coefficient, and the rolling-moment coefficient. No corrections have been applied for the effects of blocking or turbulence. Previous investigations have indicated that the effects of support-strut interference on the rolling derivatives are negligible and, therefore, no tare corrections have been applied to the data.

METHODS OF ANALYSIS

In general, the results of the investigation reported herein are analyzed in terms of the influence of the fuselage and wing on the

vertical-tail contribution to the rolling derivatives. The derivative $\left(C_{n_p}\right)_V$ has been chosen for most of the analysis since this derivative is considered to be the most important with regard to the vertical-tail contribution to the rolling derivatives.

In accordance with conventional procedures, the yawing moment due to rolling for a complete airplane can be expressed as follows:

$$C_{n_p} = \left(C_{n_p}\right)_F + \left(C_{n_p}\right)_W + \Delta_1 C_{n_p} + \left(C_{n_p}\right)_V + \Delta_2 C_{n_p} + \Delta_3 C_{n_p} \qquad (1)$$

The first three terms are concerned with the contribution of the wing-fuselage combination. The subscripts F and W refer to the contribution of the isolated fuselage and the isolated wing, respectively. These contributions together with the increment $\Delta_1 C_{n_p}$ give the contribution of the wing-fuselage combination. The increment Δ_1 is the change in the derivative caused by mutual interference of the wing and fuselage without the tail and can be obtained from test results by the following equation:

$$\Delta_1 C_{n_p} = \left(C_{n_p}\right)_{W+F} - \left[\left(C_{n_p}\right)_W + \left(C_{n_p}\right)_F\right] \qquad (2)$$

The last three terms of equation (1) are concerned with the vertical-tail contribution to the derivative. The contribution of the vertical tail when mounted on the fuselage can be determined analytically from the following equation:

$$\left(C_{n_p}\right)_V = 57.3 \frac{S_V}{S_W}\left(C_{L_\alpha}\right)_V \frac{l}{b}\left(z_V \sin\alpha + l_V \cos\alpha\right)\frac{2}{b}\left(z_V \cos\alpha - l_V \sin\alpha\right) \qquad (3)$$

In the present paper the derivatives with the subscript V indicate the effectiveness of the isolated vertical tail increased by the end-plate effect of the fuselage but without other wing and fuselage interference effects.

The wing interference with the vertical tail, indicated as the increment Δ_2, is the change in effectiveness of the vertical tail caused by addition of a wing to the fuselage-tail configuration, and can be determined from test results by the following equation:

$$\Delta_2 C_{n_p} = \left[\left(C_{n_p}\right)_{W+F+V} - \left(C_{n_p}\right)_{W+F}\right] - \left[\left(C_{n_p}\right)_{F+V} - \left(C_{n_p}\right)_{F}\right] \qquad (4)$$

The fuselage interference with the vertical tail, indicated as the increment Δ_3, is the change in effectiveness of the vertical tail caused by the fuselage interference and can be expressed as follows:

$$\Delta_3 C_{n_p} = \left[\left(C_{n_p}\right)_{F+V} - \left(C_{n_p}\right)_{F}\right] - \left(C_{n_p}\right)_{\text{Isolated tail}} \qquad (5)$$

In the preceding expression for $\Delta_3 C_{n_p}$, since no direct measurements of the term $\left(C_{n_p}\right)_{\text{Isolated tail}}$ were made, this increment was estimated with what is believed to be sufficient accuracy by equation (3) with estimated values of $\left(C_{L_\alpha}\right)_V$ from figures 17 and 18 of reference 2.

Rather than adding the increments Δ_2 and Δ_3 directly to the vertical-tail contribution determined analytically by equation (3) (as is usually done when suitable test results are available on a model similar to the airplane being considered) an attempt is made to estimate the actual vertical-tail contribution by applying corrections to the analytical expression itself. The corrections are in the form of an angle-of-attack change at $\bar{c}_V/4$ determined from the increments Δ_2 and Δ_3.

The Δ_2 increments of this investigation are converted into an average effective sidewash angle at $\bar{c}_V/4$ in terms of the wing-tip helix angle by the following relation:

$$\frac{\partial\sigma_1}{\partial\frac{pb}{2V}} = \frac{-\Delta_2 C_{n_p}}{57.3\,\frac{S_V}{S_W}\left(C_{L_\alpha}\right)_V\,\frac{1}{b}\left(z_V \sin\alpha + l_V\cos\alpha\right)} \tag{6}$$

The Δ_3 increments also are converted into an average effective sidewash angle at $\bar{c}_V/4$ in terms of the wing-tip helix angle $\frac{\partial\sigma_2}{\partial\frac{pb}{2V}}$ in a manner analogous to the one used for determining the wing sidewash angle $\frac{\partial\sigma_1}{\partial\frac{pb}{2V}}$.

The values of $\left(C_{L_\alpha}\right)_V$ used in obtaining the wing and fuselage sidewash angles from the Δ_2 and Δ_3 increments were obtained from figures 17 and 18 of reference 2 and include the end-plate effect of the fuselage.

The equations of reference 6 for calculating the vertical-tail contribution to the rolling derivatives, in terms of estimated lift-curve slope of the tail, are then modified to correct for the effects of both fuselage and wing sidewash and are as follows:

$$\left(C_{Y_p}\right)_V = -57.3\left(C_{L_\alpha}\right)_V\frac{S_V}{S_W}\left[\frac{2}{b}\left(z_V\cos\alpha - l_V\sin\alpha\right) - \left(\frac{\partial\sigma_1}{\partial\frac{pb}{2V}} + \frac{\partial\sigma_2}{\partial\frac{pb}{2V}}\right)\right] \tag{7}$$

$$\left(C_{n_p}\right)_V = 57.3\left(C_{L_\alpha}\right)_V \frac{S_V}{S_W}\frac{l}{b}\left(z_V \sin\alpha + l_V \cos\alpha\right)\left[\frac{2}{b}\left(z_V \cos\alpha - l_V \sin\alpha\right) - \left(\frac{\partial\sigma_1}{\partial\frac{pb}{2V}} + \frac{\partial\sigma_2}{\partial\frac{pb}{2V}}\right)\right] \tag{8}$$

$$\left(C_{l_p}\right)_V = -57.3\left(C_{L_\alpha}\right)_V \frac{S_V}{S_W}\frac{l}{b}\left(z_V \cos\alpha - l_V \sin\alpha\right)\left[\frac{2}{b}\left(z_V \cos\alpha - l_V \sin\alpha\right) - \left(\frac{\partial\sigma_1}{\partial\frac{pb}{2V}} + \frac{\partial\sigma_2}{\partial\frac{pb}{2V}}\right)\right] \tag{9}$$

The tail contributions calculated by using equations (7), (8), and (9) are compared with the experimental tail contributions which were obtained from the test results in the following manner: for the wing-off condition,

$$\left(C_{n_p}\right)_V = \left(C_{n_p}\right)_{F+V} - \left(C_{n_p}\right)_F$$

for the wing-on condition,

$$\left(C_{n_p}\right)_V = \left(C_{n_p}\right)_{W+F+V} - \left(C_{n_p}\right)_{W+F}$$

RESULTS AND DISCUSSION

Presentation of Results

The basic data obtained in this investigation are presented in figures 6 to 11. The longitudinal characteristics of the wing alone are presented in figure 6. The rolling characteristics of the various configurations investigated are presented in figures 7 to 11. A summary of the configurations investigated and the figures that give data for these configurations is given in table III. Most of the remaining figures (figs. 12 to 21) were made up from the data of figures 6 to 11 and present the data in a form more suitable for analysis.

Characteristics of Some Basic Configurations

Of all the basic components of the models tested, the wing is the only component for which longitudinal aerodynamic data are presented (see fig. 6). The longitudinal aerodynamic characteristics of the wing have already been discussed in reference 1 and are not discussed herein. This figure is presented since it is considered to be useful in analyzing the data.

Before entering into a discussion of the rolling derivatives, it should be pointed out that the present investigation is concerned only with the steady-state rolling derivatives and that, for the oscillatory case, additional contributions may result because of time lag and unsteady-lift effects.

A comparison of measured and calculated variation with angle of attack of the rolling derivatives for the wing alone is presented in figure 7. The methods of references 7 and 8 predict the variation with angle of attack of C_{n_p} and C_{l_p}, respectively, quite well; however, measured and calculated (reference 7) values of C_{Y_p} are in poor agreement, particularly at angles of attack above about 4°. The breaks in the curves of the rolling derivatives are partly attributed to flow separation from the wing. It is expected that, for wings with highly polished surfaces, an increase in Reynolds number would delay this flow separation to somewhat higher angles of attack.

As pointed out in reference 7, an indication of the limiting range over which flow does not separate from the wing can be obtained by locating the initial break in the plot of $C_D - \frac{C_L^2}{\pi A}$ against angle of

attack. A plot of this increment for the wing alone in figure 12 shows a break in the curve at approximately 4° angle of attack. Inspection of figures 8 to 11 for wing-on configurations shows breaks in the curves of the rolling derivatives at approximately the same angle of attack.

A comparison of wing-off and wing-on data of figures 8 to 11 shows a decrease in the vertical-tail contribution to the rolling derivatives when the wing is added to the fuselage-tail configuration. This change can be attributed to sidewash in the region of the vertical tail caused by unsymmetrical span loading on the wing due to roll (reference 6).

With the exception of vertical tail V_5, the vertical-tail contribution to C_{l_p} was rather small compared to the wing contribution because of the short distance from the center of pressure of the vertical tail to the axis of roll.

The fuselage alone generally contributes a positive increment to C_{Y_p} and C_{n_p} throughout the angle-of-attack range. These increments are small, however, in comparison with the effects of angle of attack for the other components of the models investigated.

Interference Effects

In accordance with conventional procedures, the influence of the wing and fuselage on the vertical-tail contribution to the rolling derivatives has been determined by the method of interference increments. Before going into a discussion of the various interference increments, it should be pointed out that interference increments usually are assumed to apply to airplane configurations which are somewhat similar in design to the model used in evaluating the increments. One of the factors which affects the magnitude of the interference increments is the height of the wing relative to the fuselage center line (reference 9). Since, for the present investigation, the wing was located on the fuselage center line, interference increments caused by the wing-fuselage combination are considered applicable only to midwing or near-midwing configurations. The interference increments caused by the fuselage are expected to be limited to similar fuselage-tail configurations with respect to fuselage shape and tail location.

Wing-fuselage interference.- The interference increments of the wing-fuselage combination, Δ_1 increments, are presented in figure 13 with an average curve faired through the test points of the three wing-fuselage combinations investigated. The Δ_1 increments of C_{Y_p} and C_{n_p} are rather small and do not vary appreciably with angle of attack except that

$\Delta_1 C_{n_p}$ becomes quite large at angles of attack above 16°. Interference of the wing-fuselage combinations appears to have the greatest effect on C_{l_p} for angles of attack above about 8° and tends to decrease the damping-in-roll of the combination. There was no consistent effect of fuselage length for the range of fuselage sizes investigated.

Fuselage interference on tail, wing-off.- Reference 6 has implied that fuselage sidewash at the vertical tail may influence considerably the tail contribution to the rolling derivatives at high angles of attack. The increments due to fuselage interference on the tail, Δ_3 increments, are believed to be mainly sidewash effects resulting from vortices associated with lateral forces which develop on the fuselage due to roll. The $\Delta_3 C_{n_p}$ increment occurring at $\alpha = 0°$ for some of the fuselage-tail configurations $\left(\text{difference between measured and calculated values of } \left(C_{n_p}\right)_V \text{ shown in fig. 17}\right)$ was subtracted from the data since the symmetrical fuselages tested are assumed to contribute no sidewash due to roll at 0° angle of attack. The $\Delta_3 C_{n_p}$ increments were then converted into average effective sidewash angles at $\bar{c}_V/4$ in terms of the wing-tip helix angle as mentioned previously. These results are used to derive an empirical relation for estimating the fuselage sidewash angles.

In determining this empirical relation, consideration is given to some of the factors which might be expected to influence considerably the fuselage sidewash angles such as fuselage size, distance from $\bar{c}_V/4$ to the axis of roll, and the angle of attack of the fuselage. These factors have been combined in the parameter $\frac{\Delta h}{b}$ which equals $z_V - \left(z_V \cos \alpha - l_V \sin \alpha\right)$. The values of $\frac{\partial \sigma_2}{\partial \frac{pb}{2V}}$ obtained for all the fuselage-tail configurations investigated are plotted against the parameter $\frac{\Delta h}{b}$ in figure 14 and a fitted curve is faired through the test points which can be expressed by the following equation:

$$\frac{\partial \sigma_2}{\partial \frac{pb}{2V}} = 9.30\left(\frac{\Delta h}{b}\right)^2 \qquad (10)$$

In using equation (10) to estimate $\frac{\partial \sigma_2}{\partial \frac{pb}{2V}}$ for a model having a wing span other than that of the present model ($b = 3$ ft), it should be pointed out that equation (10) must be multiplied by the ratio of the present wing span to the wing span of the model in question since the constant 9.30 was obtained from a model having $b = 3$ feet.

The squared term in equation (10) can be explained on the basis of results given in reference 10 which show that for a low-aspect-ratio wing ($A < 1$) the lift generated is a function of the angle of attack squared. Therefore, if the fuselage is treated as a low-aspect-ratio wing, the fuselage sidewash due to roll might be expected to vary as the square of the parameter $\frac{\Delta h}{b}$ since the angle of attack of the fuselage due to roll is a function of $\frac{\Delta h}{b}$.

A discussion of some of the factors affecting the agreement between measured values of fuselage sidewash and those calculated by equation (10) is given for the data plotted against angle of attack (fig. 15). Inspection of figure 15 shows that calculated values are generally in good agreement with measured values for angles of attack up to about 16° for all the fuselage-tail configurations investigated with the exception of configurations $F_2 + V_3$ and $F_3 + V_2$. Increasing the fuselage length results in an appreciable increase in the fuselage sidewash angles at high angles of attack which is predicted quite well by equation (10) since $\frac{\Delta h}{b}$ for a given angle of attack is a function of tail length. The breaks in the measured sidewash curves at high angles of attack are partly attributed to decreased lift effectiveness of the vertical tail. Reference 2 has indicated that the vertical-tail lift effectiveness may be decreased as much as 20 percent as the angle of attack is increased from 0° to 15° and that this reduction usually increases rapidly at higher angles of attack. These effects tend to increase with increasing tail length and decreasing tail span.

The tendency for equation (10) to overestimate the fuselage sidewash angles at high angles of attack for the aspect-ratio-2 tails is attributed to the fact that equation (10) does not predict the decrease in fuselage sidewash that might be expected with an increase in distance from $\bar{c}_V/4$ to the fuselage axis. An explanation of why equation (10) tends to underestimate the fuselage sidewash for angles of attack greater than about 16° but less than the angle of attack where the breaks occur in the sidewash curves for the aspect-ratio-1 tails is not known. This

indicates that factors other than those considered in equation (10) should be taken into consideration if better agreement is desired. However, in view of the generally good agreement obtained between measured and calculated values of $\left(C_{n_p}\right)_V$ (figs. 17 and 18) when corrections have been made for the effects of fuselage sidewash, equation (10) is considered to give satisfactory results.

Wing interference on tail.- Reference 6 has shown that it is necessary to correct for wing sidewash at the tail in order that good estimates of the vertical-tail contribution to the rolling derivatives be obtained even at 0° angle of attack and used actual flow surveys in the vicinity of the tail as a basis for determining this correction. Reference 6 also pointed out that for midwing or near-midwing configurations, where the wing-fuselage interference might be expected to be small, as indicated in reference 9, the Δ_2 increments at low and moderate angles of attack can be largely attributed to sidewash at the vertical tail caused by unsymmetrical span loading on the wing due to roll. Therefore, the $\Delta_2 C_{n_p}$ increments of the present investigation were converted into average effective sidewash angles at $\bar{c}_V/4$ of the vertical tail in terms of the wing-tip helix angle.

A comparison of measured values of $\frac{\partial \sigma_1}{\partial \frac{pb}{2V}}$ and theoretical values from reference 11 is shown in figure 16. With the exception of vertical tail V_2 tested in combination with fuselage F_1, the theory of reference 11 predicts the value of $\frac{\partial \sigma_1}{\partial \frac{pb}{2V}}$ at 0° angle of attack with fair accuracy, but generally does not predict the variation with angle of attack. A positive explanation for the large differences between measured and theoretical values of $\frac{\partial \sigma_1}{\partial \frac{pb}{2V}}$ at $\alpha = 0°$ for configuration $F_1 + V_2$ is not known. However, some differences might be expected since the theory is for the wing-alone case and adding a fuselage would probably have an appreciable effect on the span loading of the wing. A comparison of measured and theoretical values of wing sidewash shows good agreement for the wing-alone case (reference 11). The interference of the wing-fuselage combination might also have some effect even at 0° angle of attack.

The failure of the theory to predict the variation of $\frac{\partial \sigma_1}{\partial \frac{pb}{2V}}$ with angle of attack up to the angle of attack where the breaks occur in the sidewash curves is attributed to wing-fuselage interference and flow separation from the wing which increases with increasing angle of attack. The decrease in wing sidewash for angles of attack following the breaks in the sidewash curves is partly attributed to the decreased lift effectiveness of the vertical tail mentioned previously and to the fact that the wing is partially stalled at the higher angles of attack so that the theory is not expected to be valid (reference 11).

From the foregoing discussion and the data shown in figure 16, it appears that neglecting the theoretical variation of $\frac{\partial \sigma_1}{\partial \frac{pb}{2V}}$ with angle of attack and using the value of $\frac{\partial \sigma_1}{\partial \frac{pb}{2V}}$ at 0° angle of attack, as suggested in reference 11, will generally give the best results for estimating the wing sidewash angles throughout the angle-of-attack range.

Tail Contributions

Values of $\frac{\partial \sigma_1}{\partial \frac{pb}{2V}}$ and $\frac{\partial \sigma_2}{\partial \frac{pb}{2V}}$ which will approximate the wing and fuselage sidewash angles having been determined, it remains to be seen how well the tail contributions can be estimated by using these values in equations (7), (8), and (9) (estimated values of $\left(C_{L_\alpha}\right)_V$ from reference 2). Calculations of $\left(C_{n_p}\right)_V$ were made for the wing-off condition $\left(\frac{\partial \sigma_1}{\partial \frac{pb}{2V}} = 0\right)$ and the values obtained are compared with measured wing-off values in figure 17. The values calculated by neglecting fuselage sidewash effects are also shown for comparison. From this figure, it can be seen that accounting for the fuselage sidewash effects generally gives results which are in good agreement with measured results through the angle-of-attack range, and the agreement is considerably better than when the fuselage sidewash is neglected. The two methods give the same

values at 0° angle of attack, of course, because it is assumed that fuselage sidewash is zero $\left(\frac{\partial \sigma_2}{\partial \frac{pb}{2V}} = 0\right)$ at 0° angle of attack.

Calculations of $\left(C_{n_p}\right)_V$ were made for the wing-on condition and these values are compared with measured wing-on values in figure 18. The calculations were made by using theoretical values of $\frac{\partial \sigma_1}{\partial \frac{pb}{2V}}$ from reference 11 but neglecting fuselage sidewash effects $\left(\frac{\partial \sigma_2}{\partial \frac{pb}{2V}} = 0\right)$. The calculated and measured values of $\left(C_{n_p}\right)_V$ are generally in good agreement at 0° angle of attack but, as was expected, show considerable error at moderate and high angles of attack since the fuselage sidewash effects were neglected.

Calculations taking into account both fuselage and wing sidewash effects were made and are compared in the same figure. The good agreement obtained at moderate and high angles of attack indicates that the empirical equation for estimating $\frac{\partial \sigma_2}{\partial \frac{pb}{2V}}$ (which was determined from wing-off data) applies to both wing-off and wing-on configurations.

A comparison of the wing-off and wing-on data of figures 17 and 18 at 0° angle of attack gives an indication of the magnitude by which wing sidewash changes $\left(C_{n_p}\right)_V$. For example, adding the wing to $F_2 + V_2$ decreased the measured value of $\left(C_{n_p}\right)_V$ by an increment of 0.022. The theoretical correction for wing sidewash results in a decrease in $\left(C_{n_p}\right)_V$ by an increment of 0.018 or about 82 percent of the measured decrease.

Since the effects of fuselage and wing sidewash on the vertical-tail contribution to the rolling derivatives has been confined to $\left(C_{n_p}\right)_V$, it remains to be seen how well $\left(C_{Y_p}\right)_V$ and $\left(C_{l_p}\right)_V$ can be estimated by using the fuselage and wing sidewash corrections. A comparison of measured and calculated values of $\left(C_{Y_p}\right)_V$, $\left(C_{n_p}\right)_V$, and $\left(C_{l_p}\right)_V$ for the

three fuselages investigated when tested in combination with vertical tail V_2 in figure 19 generally shows good agreement throughout the angle-of-attack range. It is of interest to note that although the corrections for fuselage and wing sidewash were determined from $\left(C_{n_p}\right)_V$, they can be used to calculate $\left(C_{Y_p}\right)_V$ and $\left(C_{l_p}\right)_V$ with approximately equal accuracy.

The validity of the method used herein for estimating the vertical-tail contribution to the rolling derivatives is checked by comparing calculated values of the derivatives with measured values taken from reference 12 (fig. 20) and from some unpublished data (fig. 21) for other models. The data shown in figure 20 are for a midwing model having 45° sweptback wing and tail surfaces, aspect ratio of 2.31, taper ratio of 1.0, and a circular-arc fuselage of fineness ratio 8.34. The data shown in figure 21 are for a near-midwing semitailless model having 41.57° sweptback wing and tail surfaces, wing aspect ratio of 3.60, tail aspect ratio of 2.54, and a fuselage of fineness ratio 5.05. Calculated and measured values of the rolling derivatives for the 45° sweptback midwing model are in good agreement as expected since this model and the model used to determine the fuselage sidewash correction are similar in design, differing mainly in wing aspect ratio and taper ratio (fig. 20). Calculated and measured values of the rolling derivatives for the near-midwing semitailless model are also in good agreement as shown in figure 21.

From the foregoing discussion and the data shown in figures 20 and 21, it appears that the method used herein for estimating the vertical-tail contribution to the rolling derivatives can be expected to give good results for airplane configurations similar to the models investigated.

CONCLUSIONS

The results of an investigation to determine the influence of the wing and fuselage on the vertical-tail contribution to the rolling derivatives of midwing airplane models with 45° sweptback surfaces have led to the following conclusions:

1. The vertical-tail contribution to the rolling derivatives of midwing or near-midwing configurations can be calculated with good accuracy throughout the angle-of-attack range by using available procedures when corrections have been made for the effects of fuselage and wing sidewash at the tail due to roll.

2. The mutual wing-fuselage interference increments of the wing-fuselage configurations investigated showed no consistent effect of fuselage length. The increments were usually rather small and did not vary appreciably with angle of attack except that the increment in yawing moment due to rolling became quite large at angles of attack above 16°.

3. The contribution of the fuselage alone to the rolling derivatives was small in comparison with the effects of angle of attack for the other components of the models investigated.

Langley Aeronautical Laboratory
National Advisory Committee for Aeronautics
Langley Field, Va., September 14, 1951

REFERENCES

1. Brewer, Jack D., and Lichtenstein, Jacob H.: Effect of Horizontal Tail on Low-Speed Static Lateral Stability Characteristics of a Model Having 45° Sweptback Wing and Tail Surfaces. NACA TN 2010, 1950.

2. Queijo, M. J., and Wolhart, Walter D.: Experimental Investigation of the Effect of Vertical-Tail Size and Length and of Fuselage Shape and Length on the Static Lateral Stability Characteristics of a Model with 45° Sweptback Wing and Tail Surfaces. NACA TN 2168, 1950.

3. Letko, William: Effect of Vertical-Tail Area and Length on the Yawing Stability Characteristics of a Model Having a 45° Sweptback Wing. NACA TN 2358, 1951.

4. Recant, Isidore G., and Wallace, Arthur R.: Wind-Tunnel Investigation of Effect of Yaw on Lateral Stability Characteristics. III - Symmetrically Tapered Wing at Various Positions on Circular Fuselage with and without a Vertical Tail. NACA TN 825, 1941.

5. MacLachlan, Robert, and Letko, William: Correlation of Two Experimental Methods of Determining the Rolling Characteristics of Unswept Wings. NACA TN 1309, 1947.

6. Letko, William, and Riley, Donald R.: Effect of an Unswept Wing on the Contribution of Unswept-Tail Configurations to the Low-Speed Static- and Rolling-Stability Derivatives of a Midwing Airplane Model. NACA TN 2175, 1950.

7. Goodman, Alex, and Fisher, Lewis R.: Investigation at Low Speeds of the Effect of Aspect Ratio and Sweep on Rolling Stability Derivatives of Untapered Wings. NACA Rep. 968, 1950. (Formerly NACA TN 1835.)

8. Goodman, Alex, and Adair, Glenn H.: Estimation of the Damping in Roll of Wings through the Normal Flight Range of Lift Coefficient. NACA TN 1924, 1949.

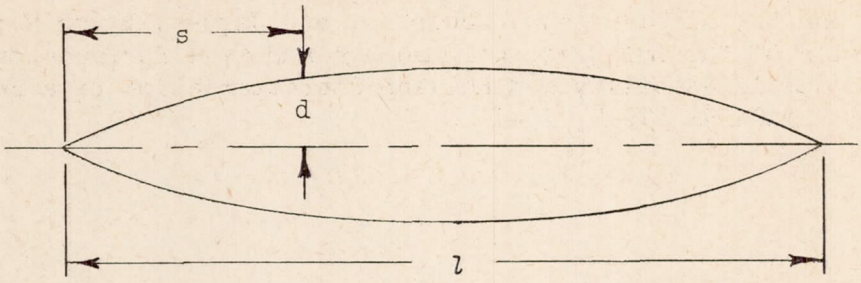
9. Recant, Isidore G., and Wallace, Arthur R.: Wind-Tunnel Investigation of the Effect of Vertical Position of the Wing on the Side Flow in the Region of the Vertical Tail. NACA TN 804, 1941.

10. Bollay, William: A Non-Linear Wing Theory and Its Application to Rectangular Wings of Small Aspect Ratio. Z.f.a.M.M., Bd. 19, Nr. 1, Feb. 1939, pp. 21-35.

11. Michael, William H., Jr.: Analysis of the Effects of Wing Interference on the Tail Contributions to the Rolling Derivatives. NACA TN 2332, 1951.

12. Bird, John D., Lichtenstein, Jacob H., and Jaquet, Byron M.: Investigation of the Influence of Fuselage and Tail Surfaces on Low-Speed Static Stability and Rolling Characteristics of a Swept-Wing Model. NACA RM L7H15, 1947.

TABLE I.- FUSELAGE COORDINATES



s/l	d/l for -		
	Fuselage 1	Fuselage 2	Fuselage 3
0	0	0	0
.025	.010	.007	.005
.050	.020	.014	.010
.075	.029	.021	.014
.100	.037	.027	.018
.125	.045	.033	.022
.150	.052	.039	.026
.200	.065	.048	.032
.250	.076	.057	.038
.30	.085	.063	.042
.35	.091	.068	.046
.40	.096	.072	.048
.45	.099	.074	.049
.50	.100	.075	.050
.55	.099	.074	.049
.60	.096	.072	.048
.65	.091	.068	.046
.70	.085	.063	.042
.75	.076	.057	.038
.80	.065	.048	.032
.85	.052	.039	.026
.90	.037	.027	.018
.95	.020	.014	.010
1.00	0	0	0

NACA

TABLE II.- GEOMETRIC CHARACTERISTICS OF MODEL

Wing:	
Aspect ratio, A_W	4.0
Taper ratio, λ_W	0.6
Quarter-chord sweep angle, Λ_W, deg	45
Dihedral angle, deg	0
Twist, deg	0
NACA airfoil section	65A008
Area, S_W, sq ft	2.25
Span, b_W, ft	3.00
Mean chord, $\bar{c}_W$, ft	0.756

Fuselage:	F_1	F_2	F_3
Length, ft	2.50	3.34	5.00
Fineness ratio	5.00	6.67	10.00
Tail length, l_V, ft (all tails)	1.04	1.39	2.09
Tail-length ratio, l_V/b_W, (all tails)	0.347	0.464	0.697

Vertical tail:	V_1	V_2	V_3	V_4	V_5
Aspect ratio, A_V	1.0	1.0	1.0	2.0	2.0
Taper ratio	0.6	0.6	0.6	0.6	0.6
Quarter-chord sweep angle, Λ_V, deg	45	45	45	45	45
NACA airfoil section	65A008	65A008	65A008	65A008	65A008
Area, S_V, sq ft	0.169	0.338	0.506	0.338	0.675
Span, b_V, ft	0.408	0.583	0.710	0.825	1.159
Mean chord, $\bar{c}_V$, ft	0.417	0.592	0.725	0.416	0.592
Perpendicular distance from fuselage center line to $\bar{c}_V/4$ of vertical tail, z_V, ft	0.192	0.267	0.325	0.375	0.532

TABLE III.- CONFIGURATIONS INVESTIGATED

Wing off		Wing on	
Configuration (a)	Figure	Configuration (a)	Figure
-------	-----	W	6, 7
F_1 $F_1 + V_2$ $F_1 + V_4$	8(a)	$W + F_1$ $W + F_1 + V_2$ $W + F_1 + V_4$	8(b)
F_2 $F_2 + V_1$ $F_2 + V_2$ $F_2 + V_3$	9(a)	$W + F_2$ $W + F_2 + V_1$ $W + F_2 + V_2$ $W + F_2 + V_3$	9(b)
$F_2 + V_4$ $F_2 + V_5$	10(a)	$W + F_2 + V_4$ $W + F_2 + V_5$	10(b)
F_3 $F_3 + V_2$ $F_3 + V_4$	11(a)	$W + F_3$ $W + F_3 + V_2$ $W + F_3 + V_4$	11(b)

[a]Notation (For details, see table II and figs. 2 to 4):

W wing
F fuselage
V vertical tail

NACA

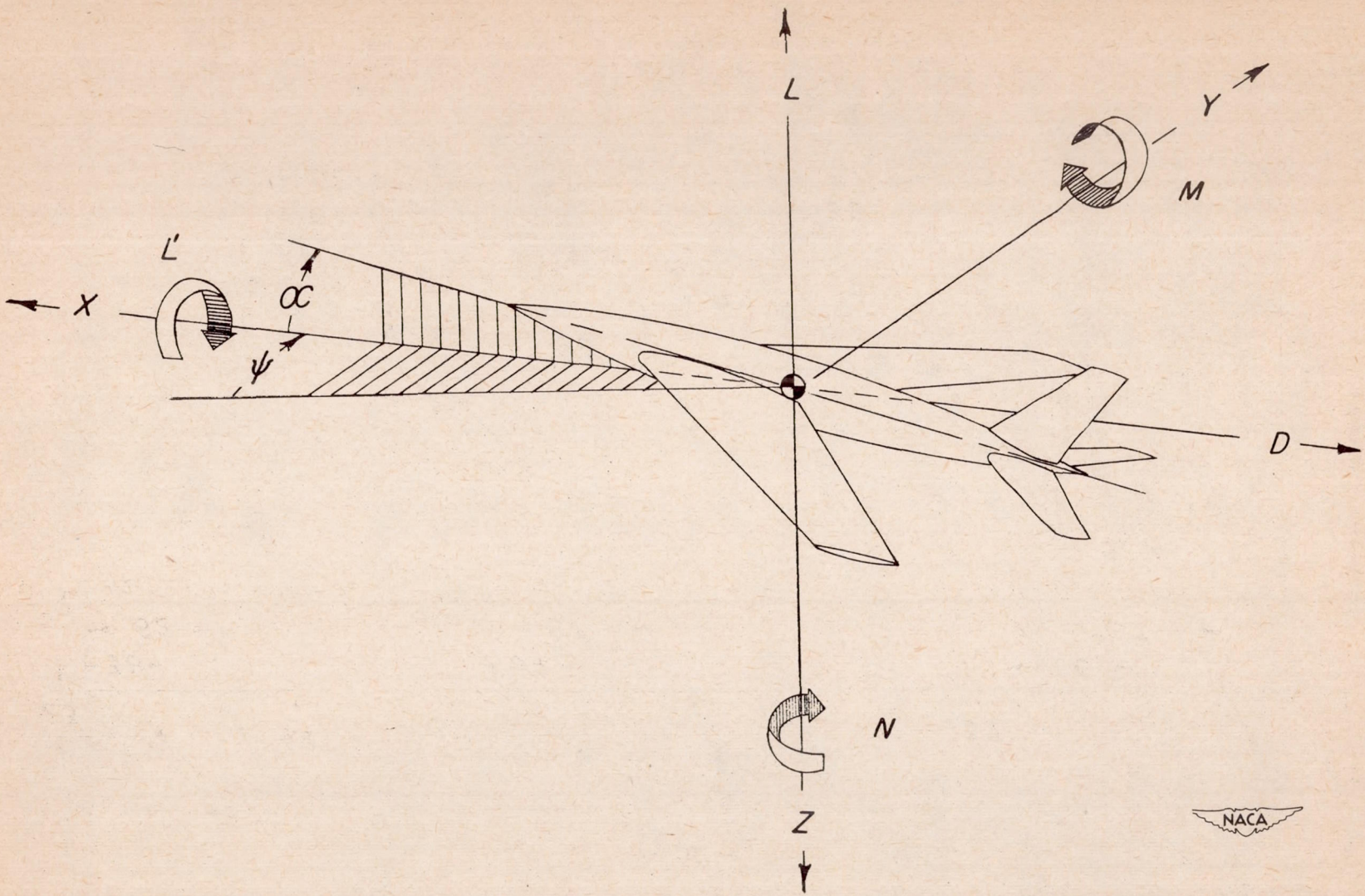
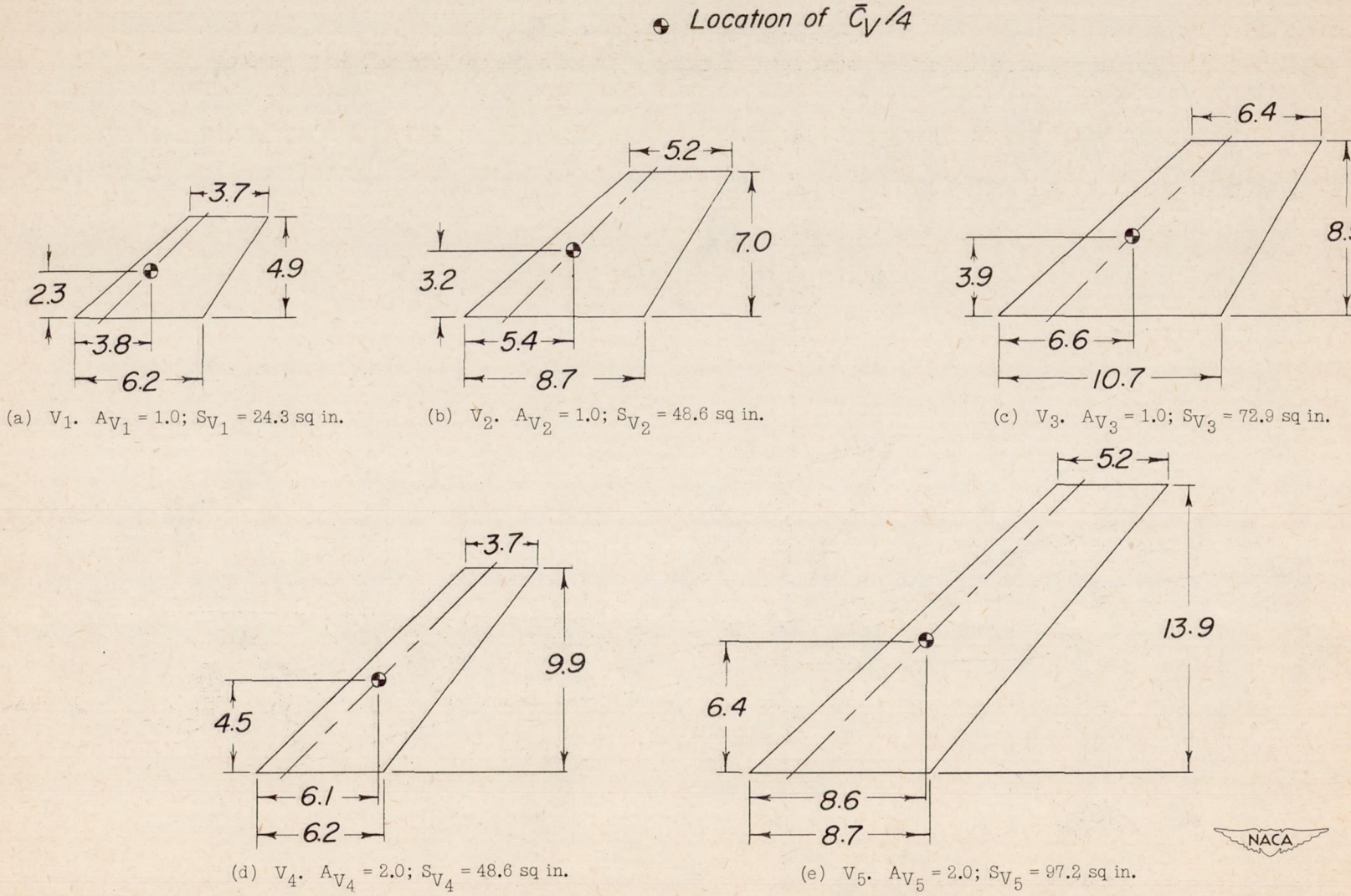


Figure 1.- System of axes used. Arrows indicate positive direction of angles, forces, and moments.



(a) V_1. $A_{V_1} = 1.0$; $S_{V_1} = 24.3$ sq in.

(b) V_2. $A_{V_2} = 1.0$; $S_{V_2} = 48.6$ sq in.

(c) V_3. $A_{V_3} = 1.0$; $S_{V_3} = 72.9$ sq in.

(d) V_4. $A_{V_4} = 2.0$; $S_{V_4} = 48.6$ sq in.

(e) V_5. $A_{V_5} = 2.0$; $S_{V_5} = 97.2$ sq in.

Figure 2.- Dimensions of vertical tails tested. $\lambda = 0.6$; $\Lambda = 45^\circ$; profile, NACA 65A008. All dimensions are in inches.

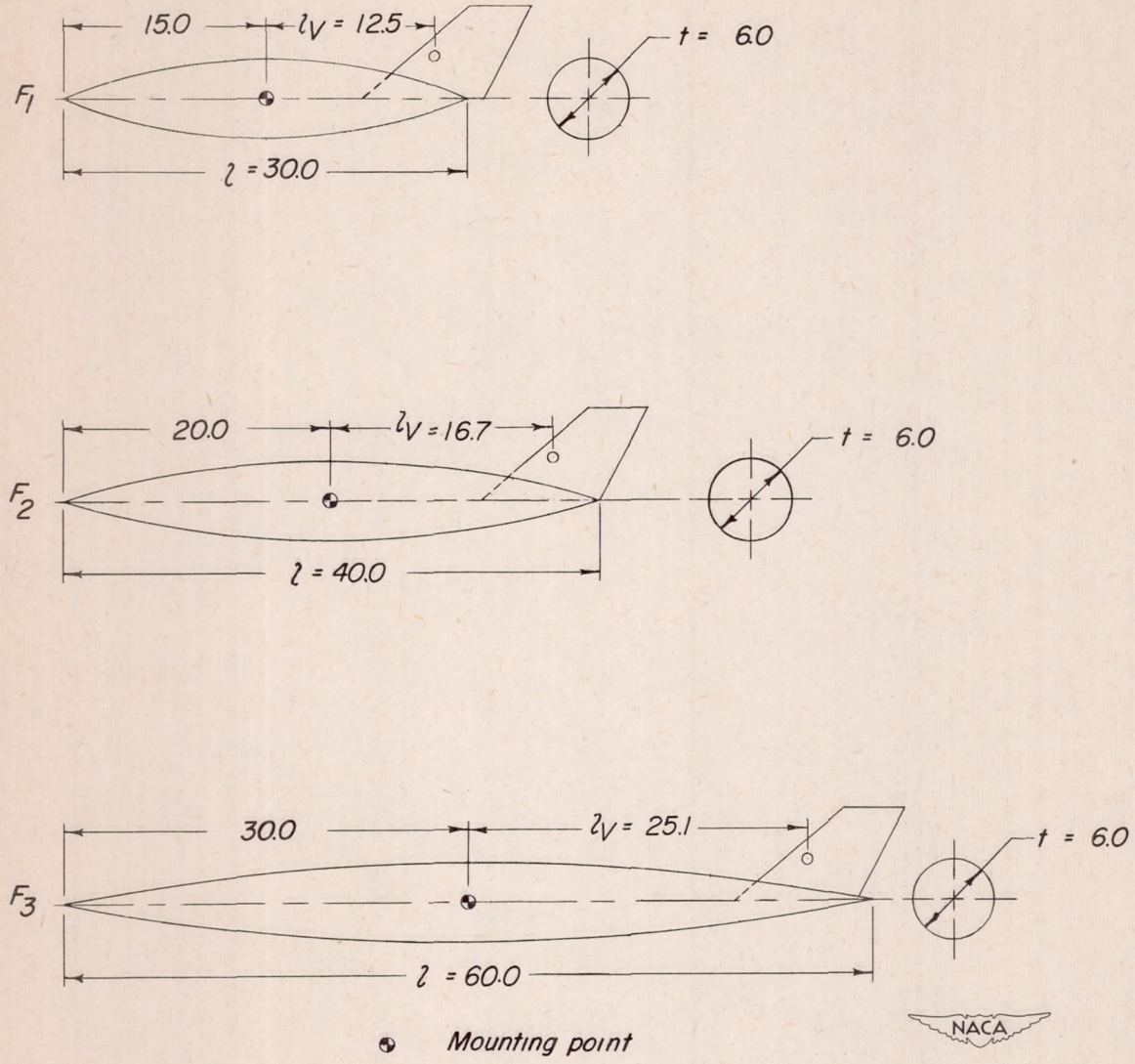


Figure 3.- Dimensions of fuselages tested; profile ordinates in table I. All dimensions are in inches.

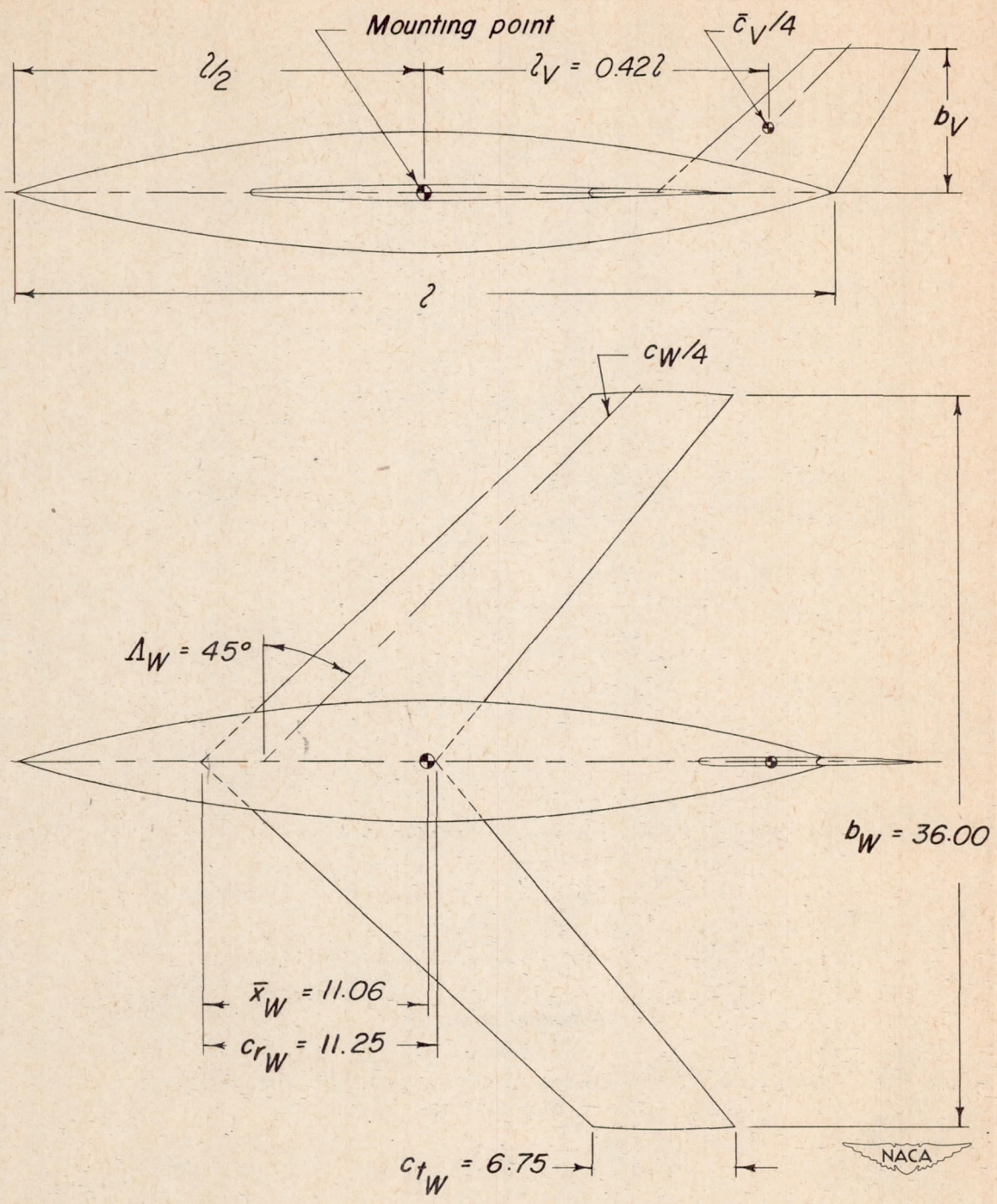


Figure 4.- Dimensions and location of wing and vertical tails. All dimensions are in inches.

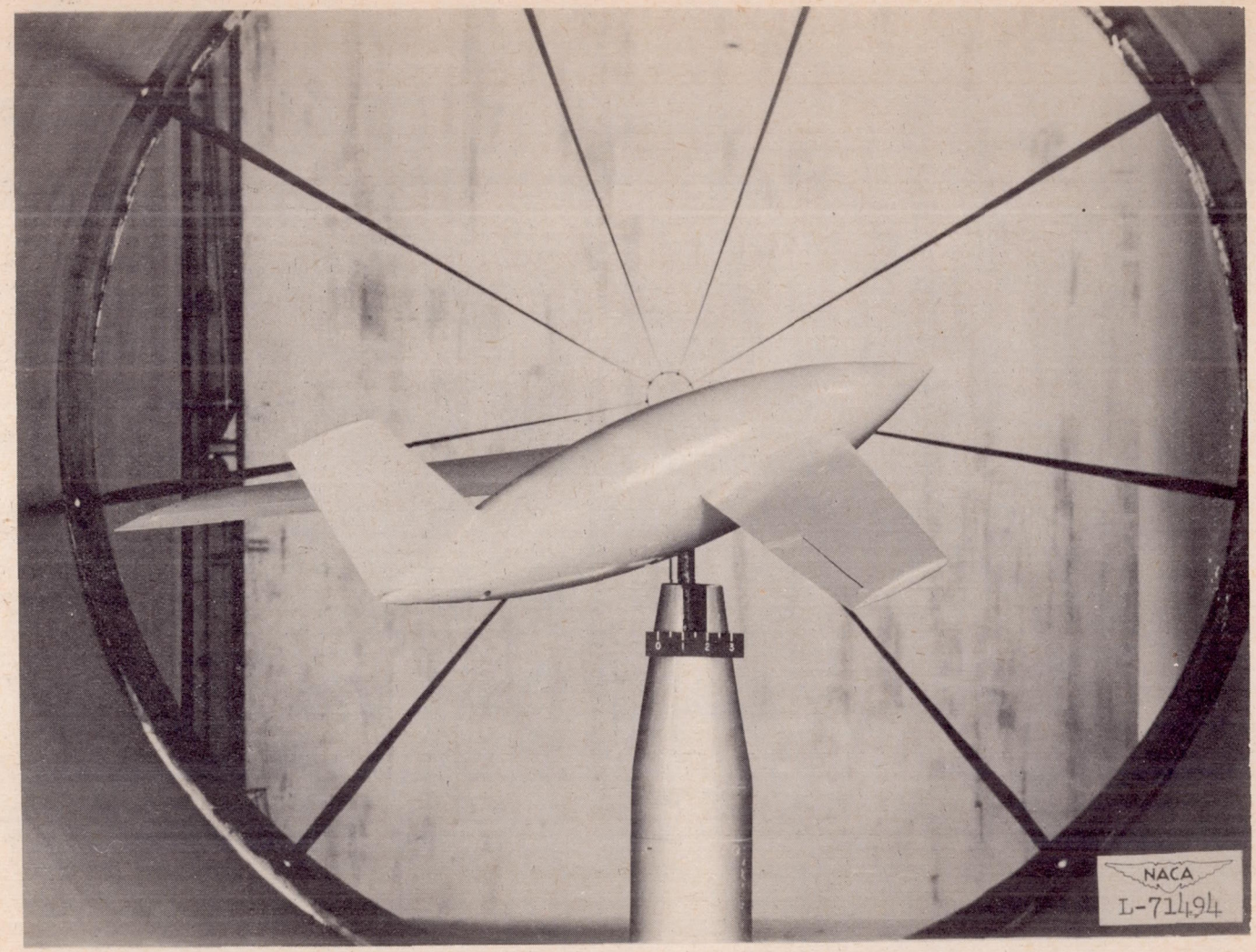


Figure 5.- View of model, configuration W + F_2 + V_2, mounted in the 6-foot-diameter rolling-flow test section of the Langley stability tunnel.

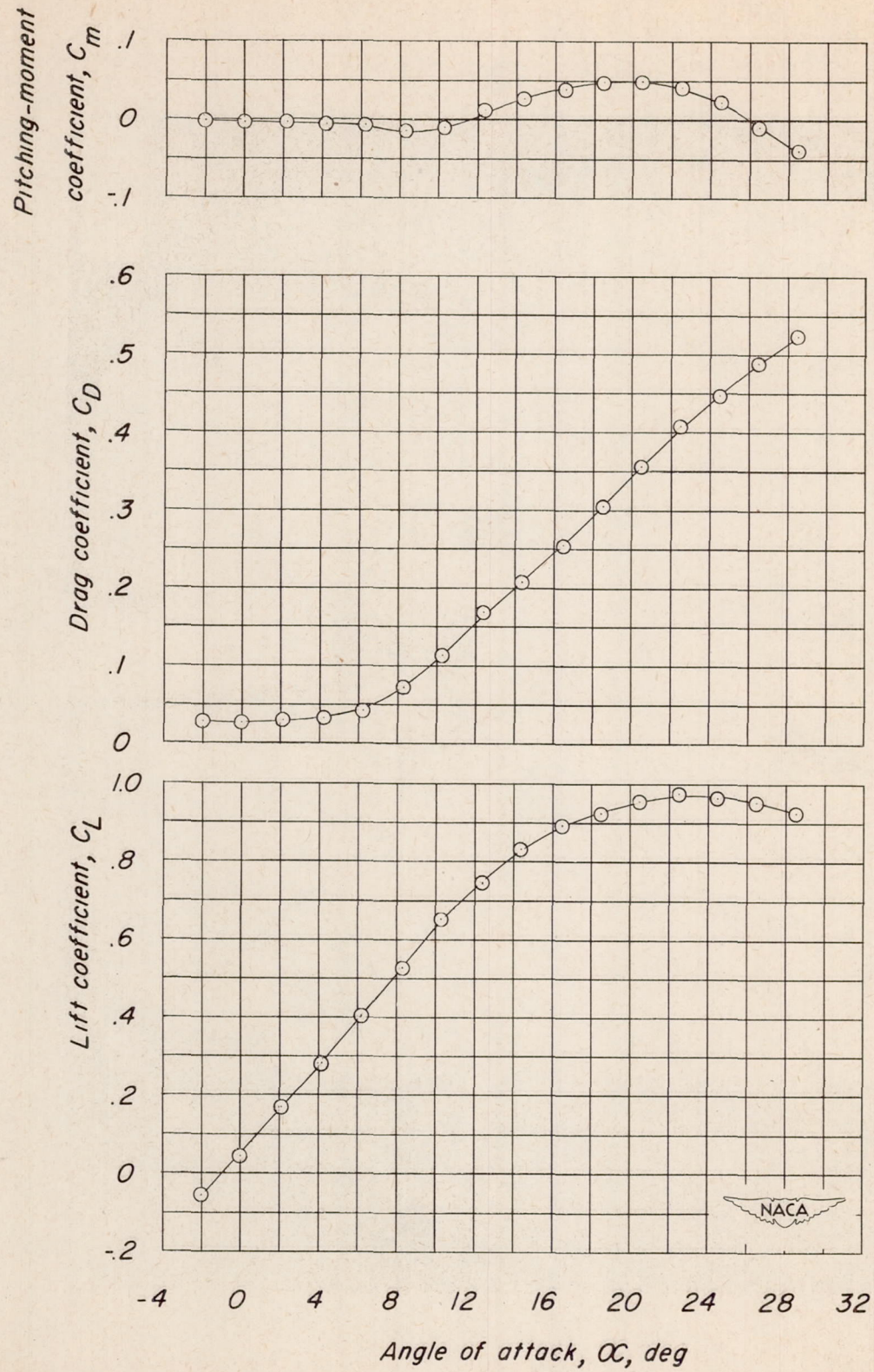


Figure 6.- Static longitudinal stability characteristics of the wing.

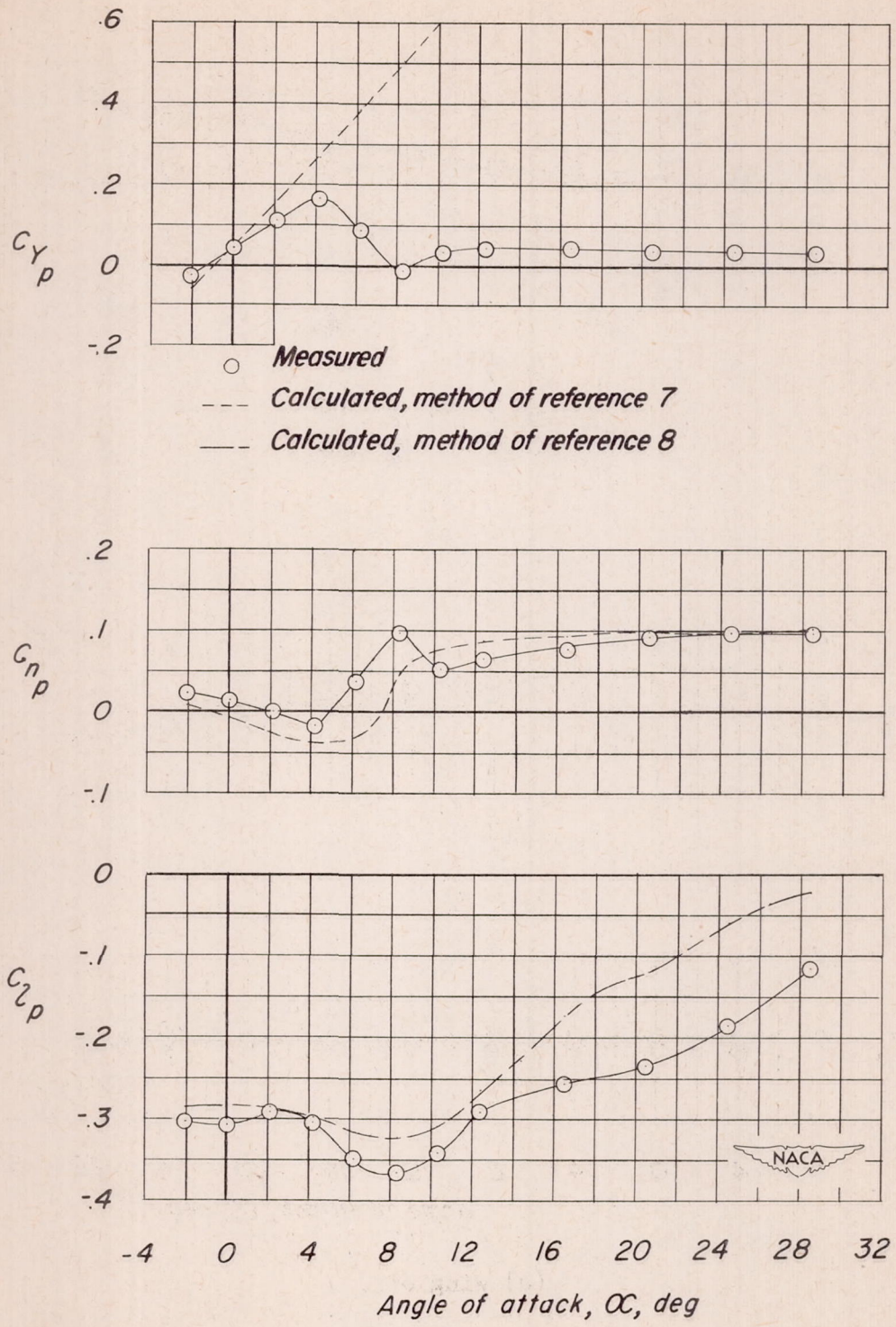
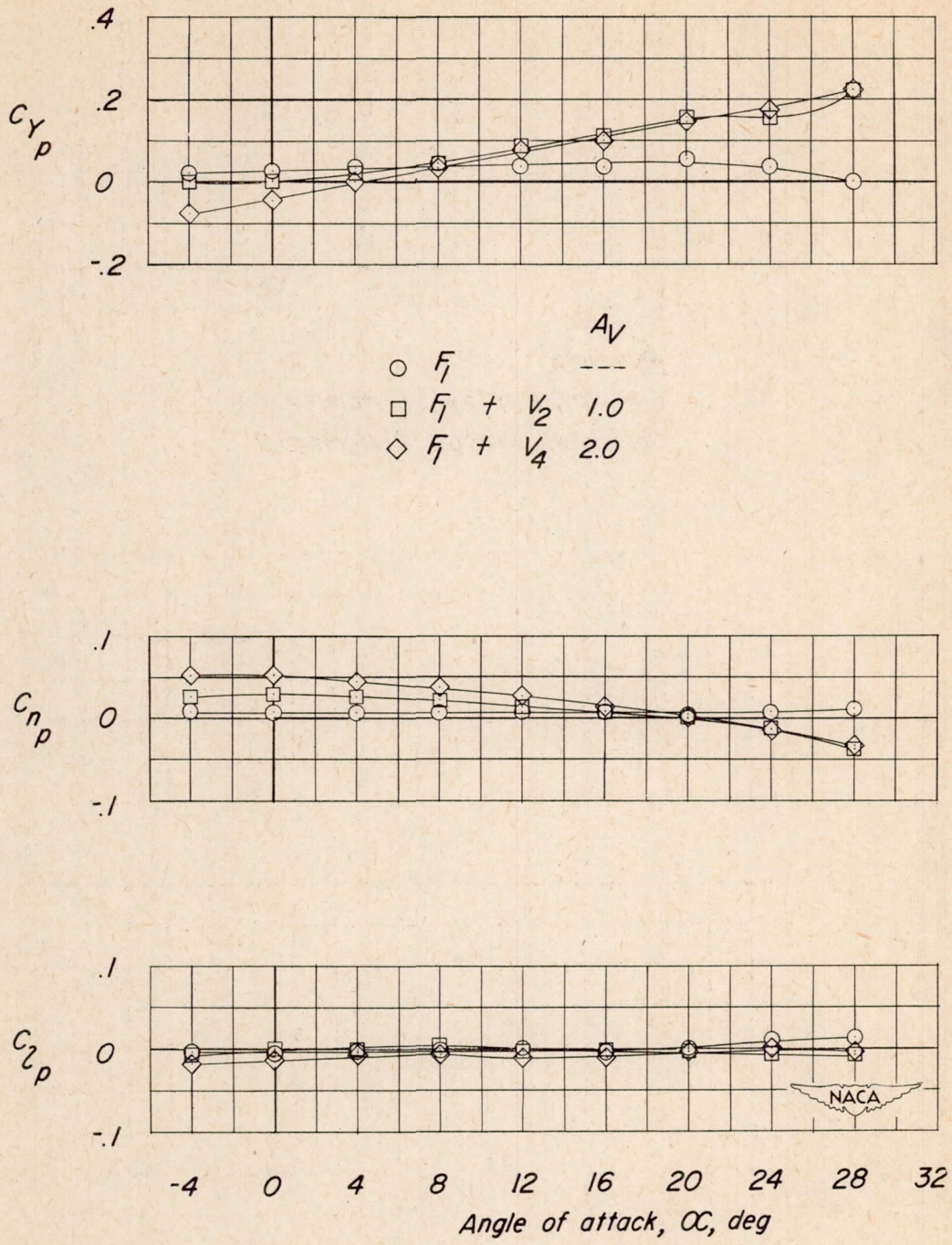
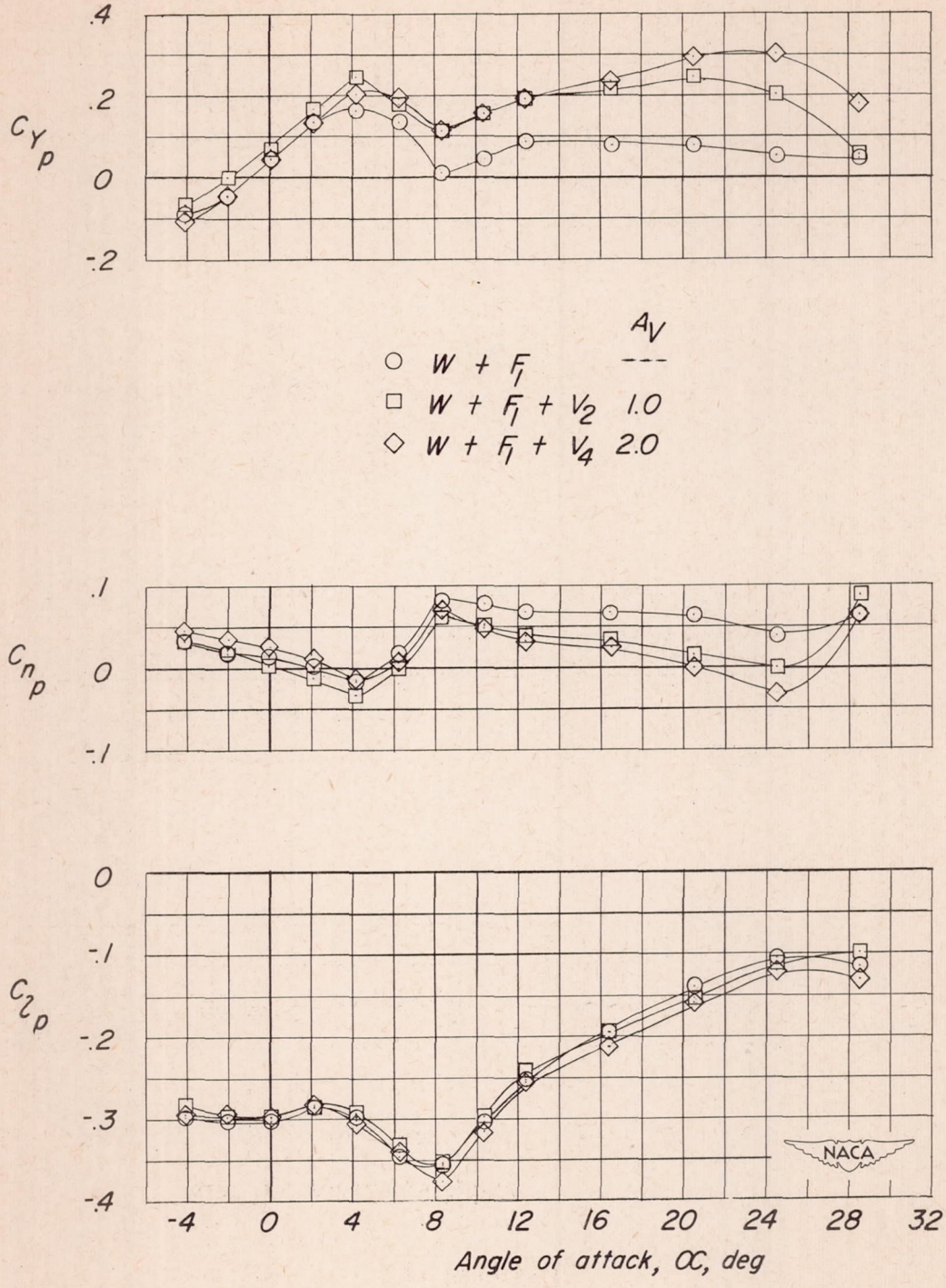


Figure 7.- Comparison of measured and calculated variation with angle of attack of C_{Y_p}, C_{n_p}, and C_{l_p} for the wing alone.



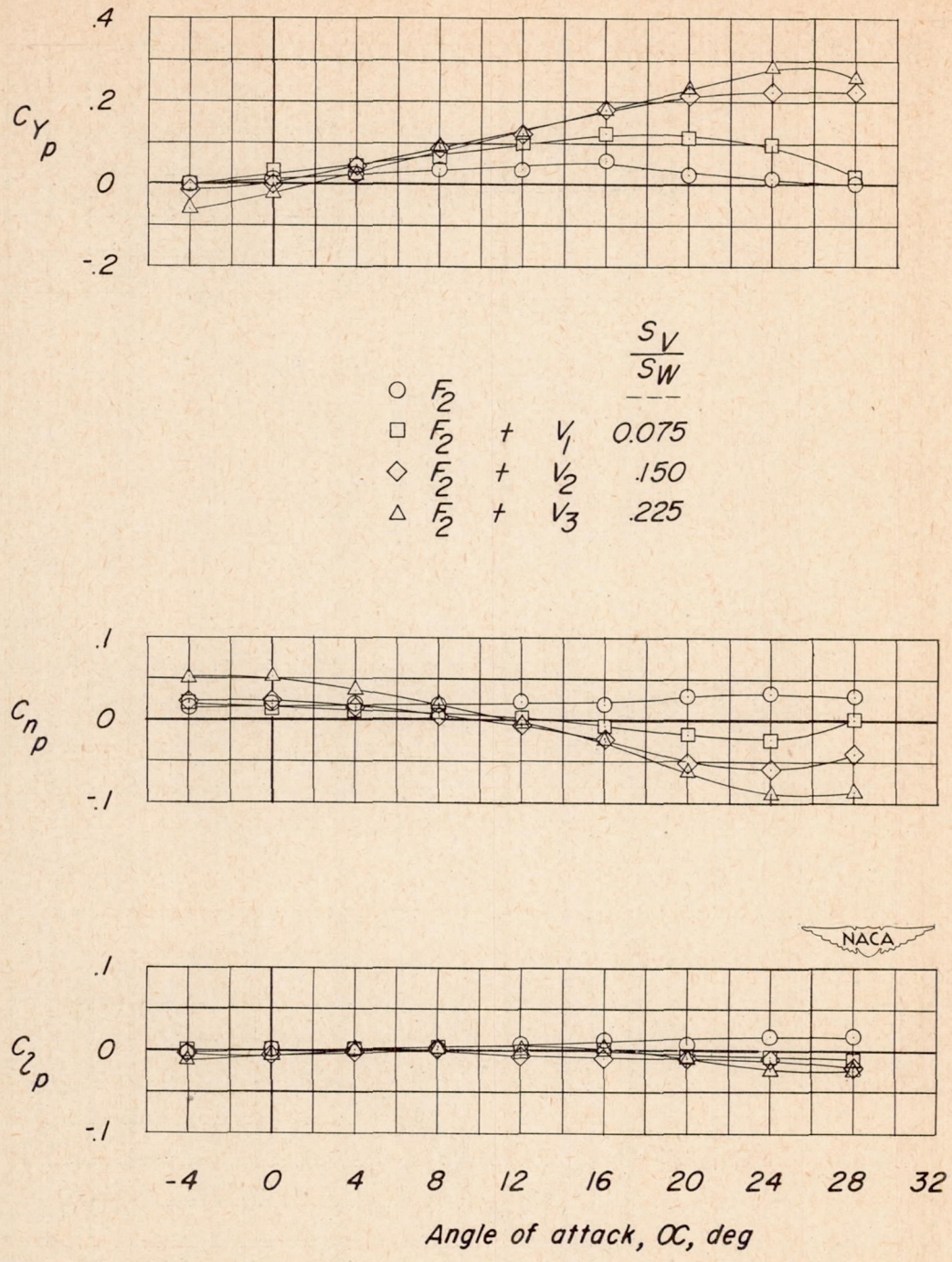
(a) Wing off.

Figure 8.- Variation with angle of attack of C_{Y_p}, C_{n_p}, and C_{l_p} for fuselage F_1. $\frac{S_V}{S_W} = 0.150$.



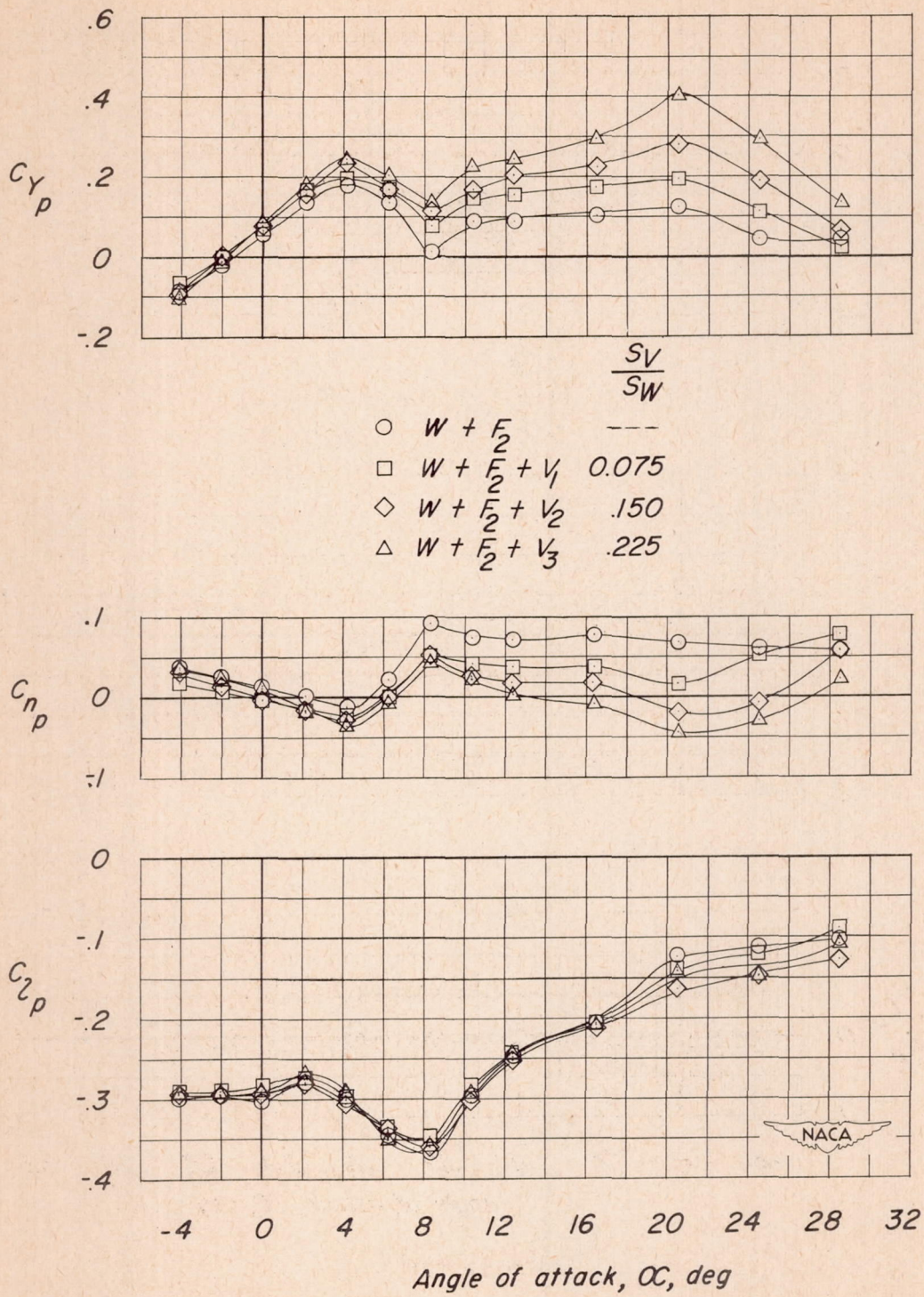
(b) Wing on.

Figure 8.- Concluded.



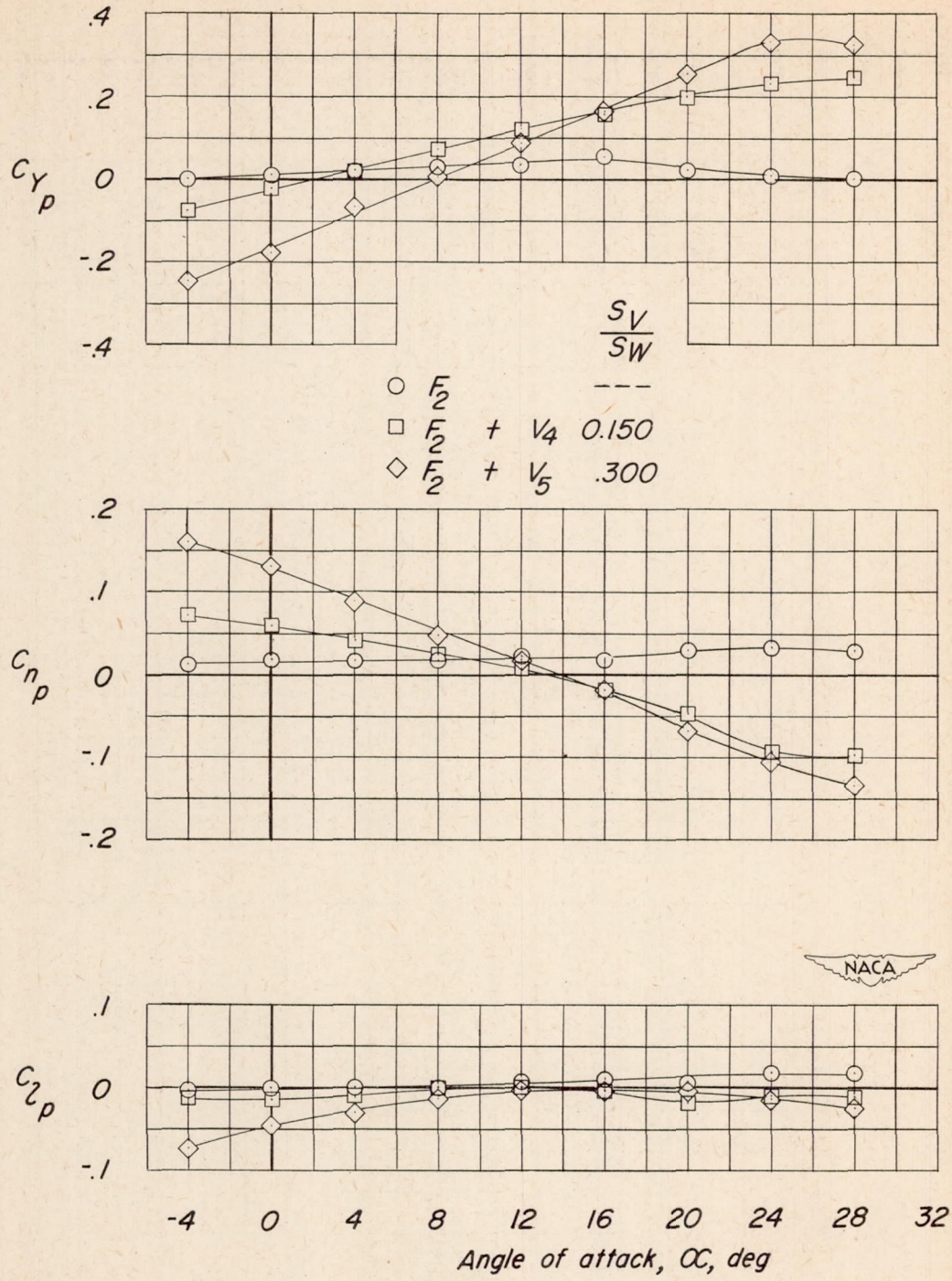
(a) Wing off.

Figure 9.- Variation with angle of attack of C_{Y_p}, C_{n_p}, and C_{l_p} for fuselage F_2. A_V = 1.0.



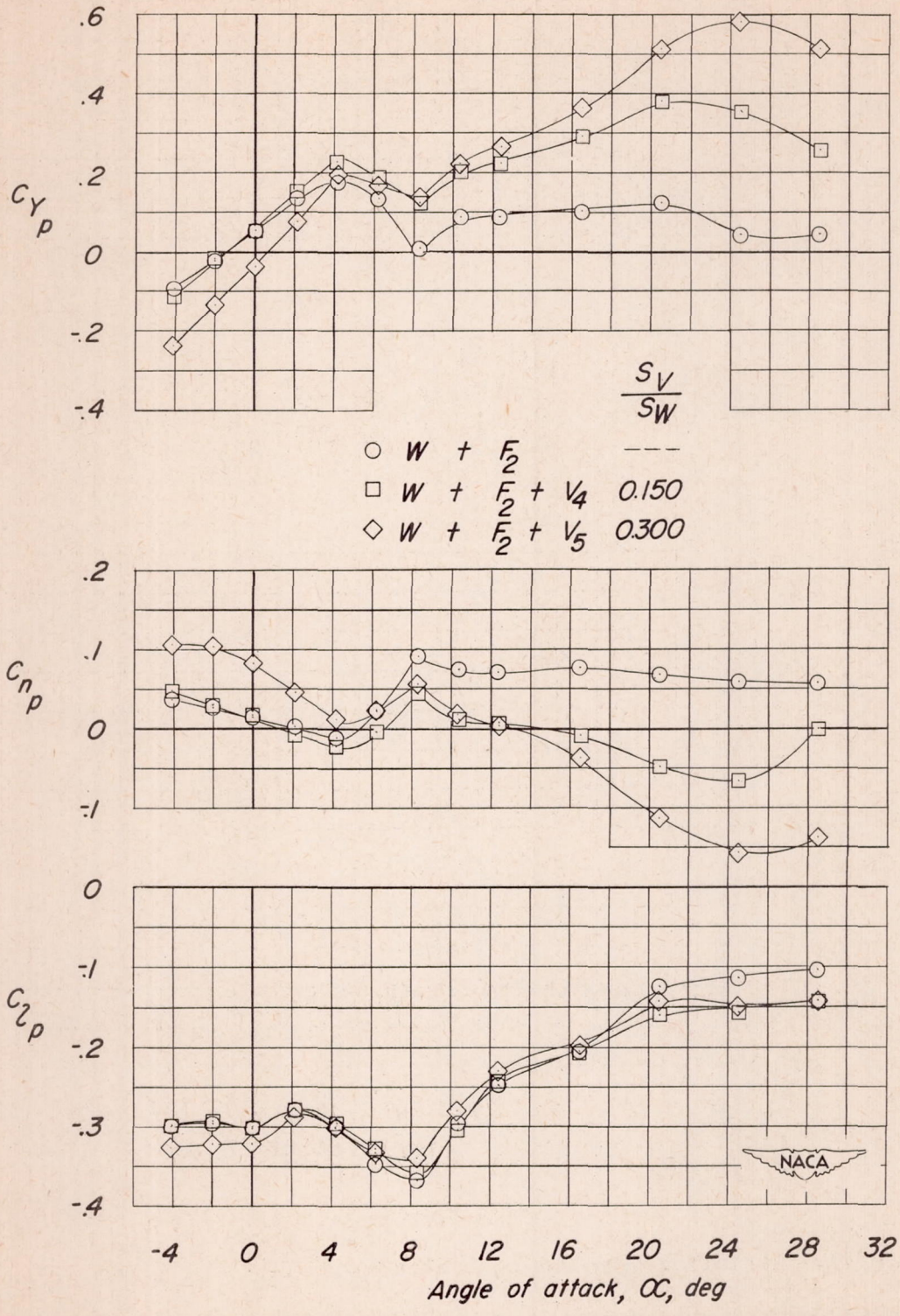
(b) Wing on.

Figure 9.- Concluded.



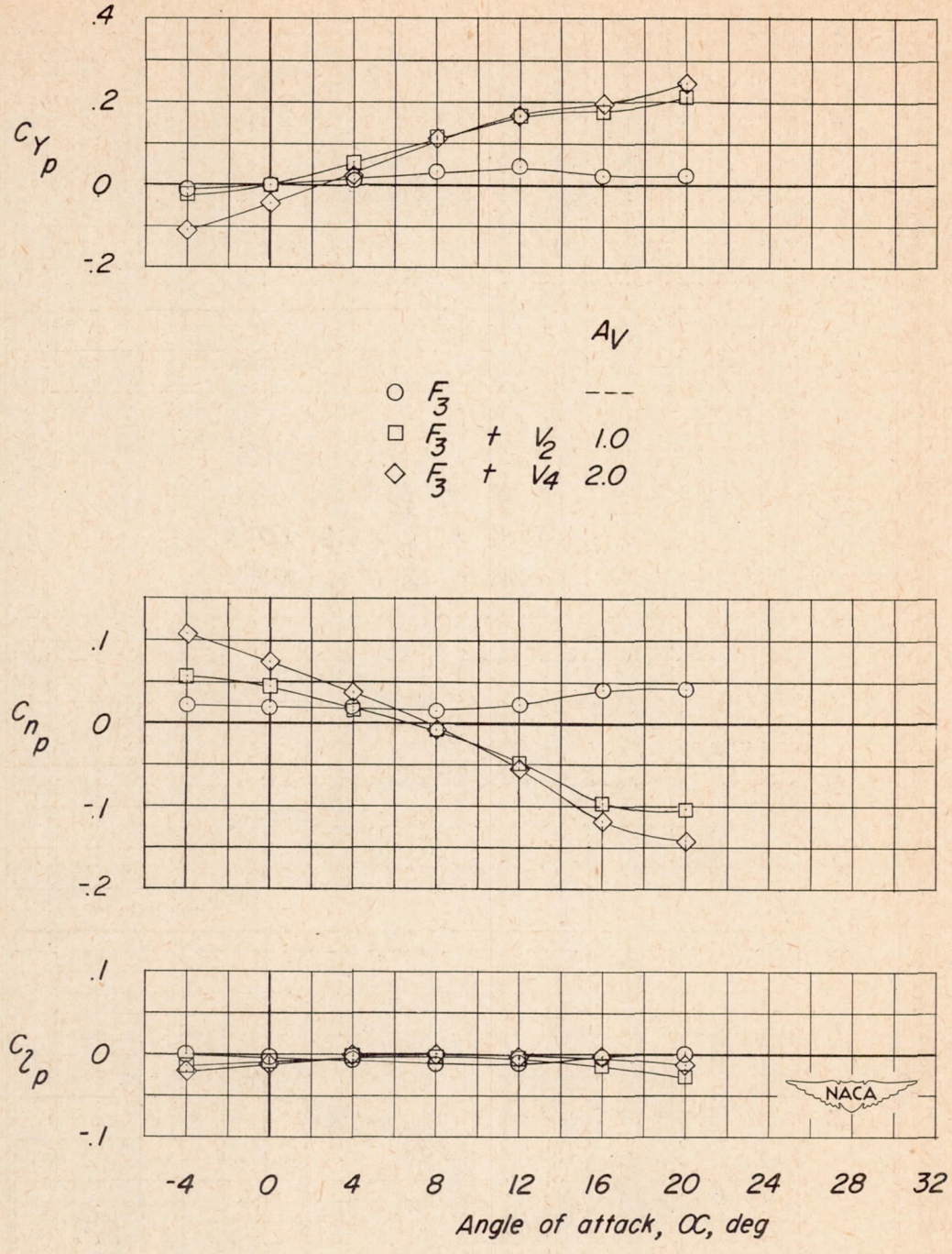
(a) Wing off.

Figure 10.- Variation with angle of attack of C_{Y_p}, C_{n_p}, and C_{l_p} for fuselage F_2. A_V = 2.0.



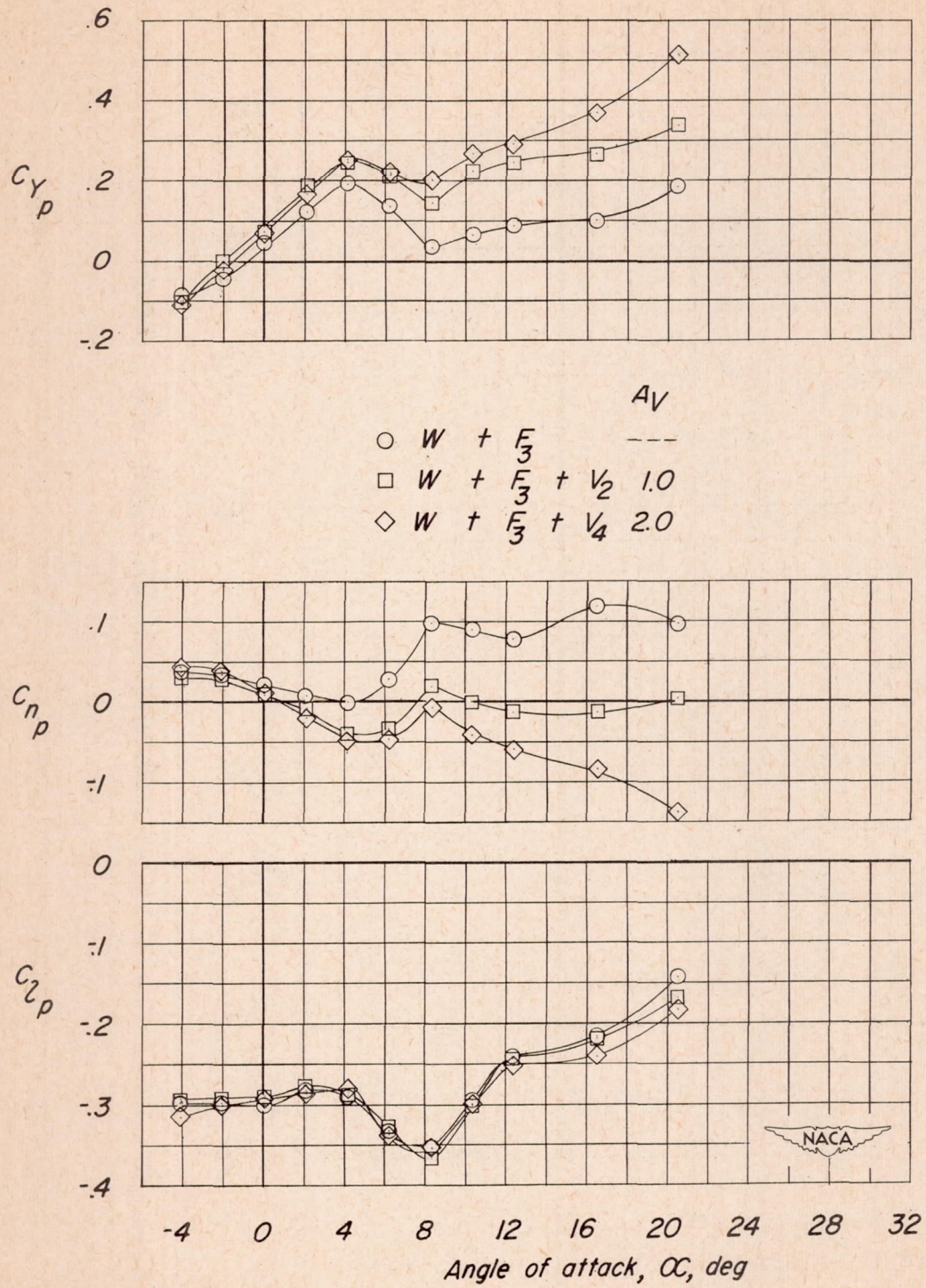
(b) Wing on.

Figure 10.- Concluded.



(a) Wing off.

Figure 11.- Variation with angle of attack of C_{Y_p}, C_{n_p}, and C_{l_p} for fuselage F_3. $\frac{S_V}{S_W} = 0.150$.



(b) Wing on.

Figure 11.- Concluded.

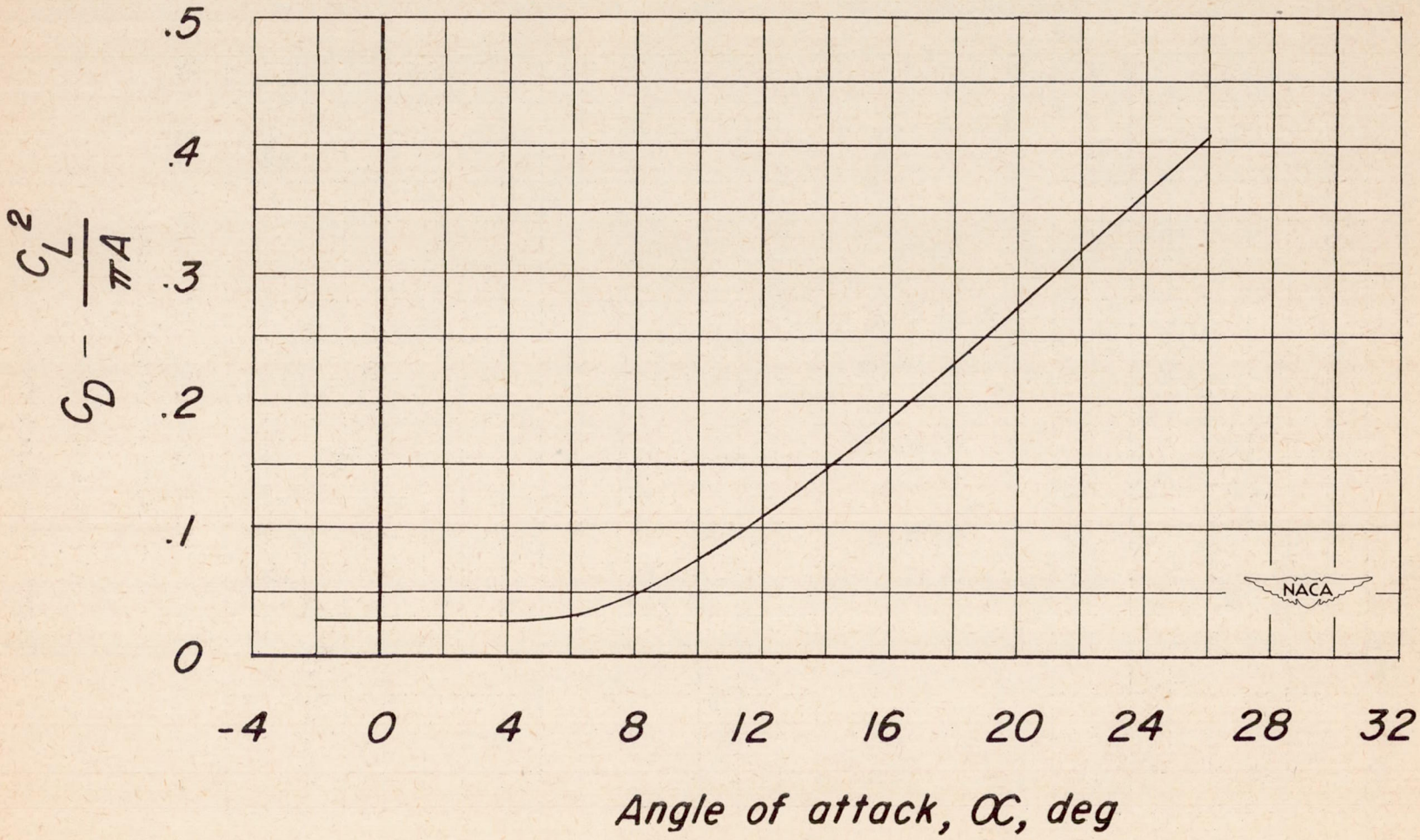


Figure 12.- Variation with angle of attack of $C_D - \frac{C_L^2}{\pi A}$ for 45° swept-back wing.

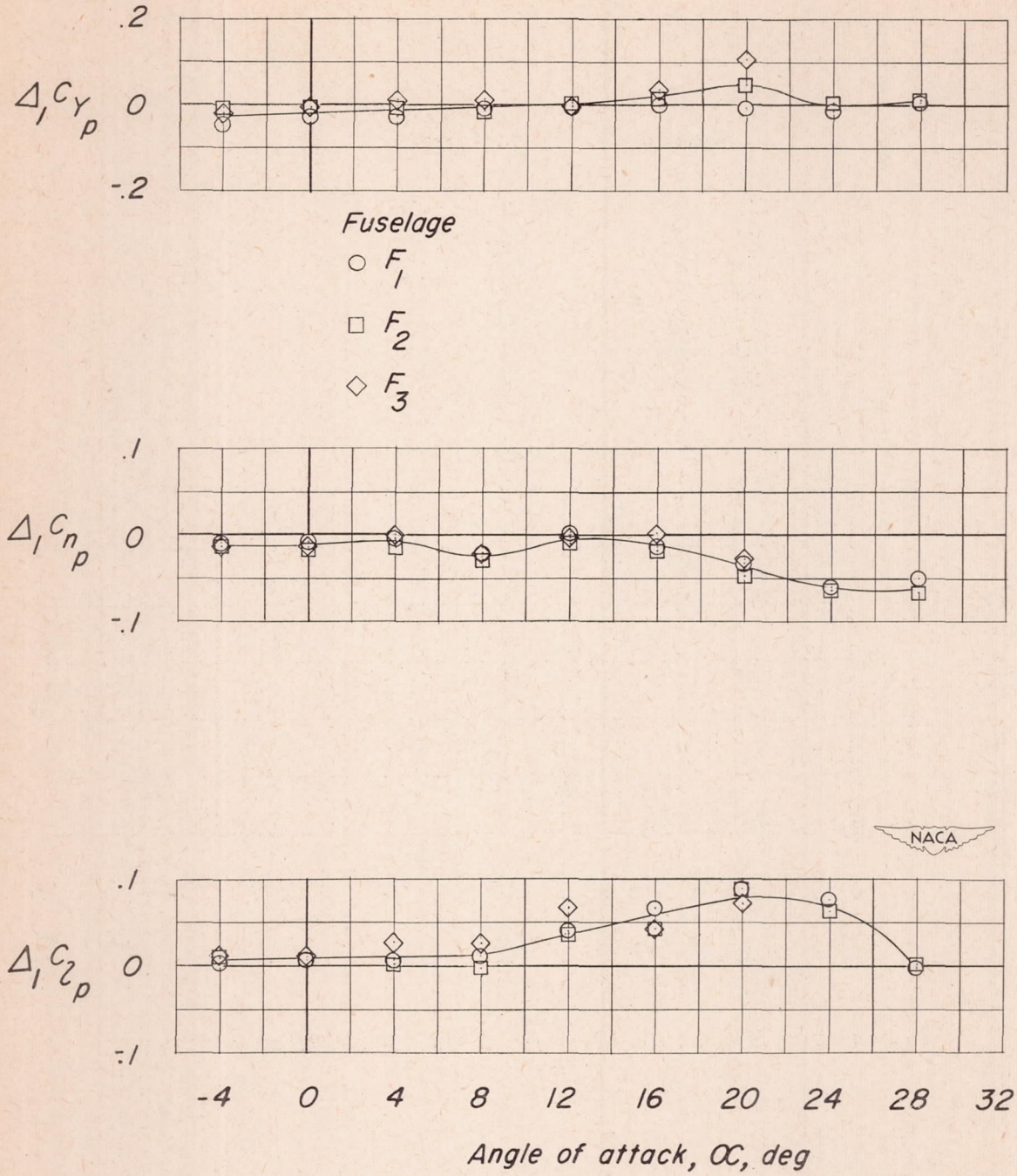


Figure 13.- Variation of increments of C_{Y_p}, C_{n_p}, and C_{l_p} caused by wing-fuselage interference with angle of attack.

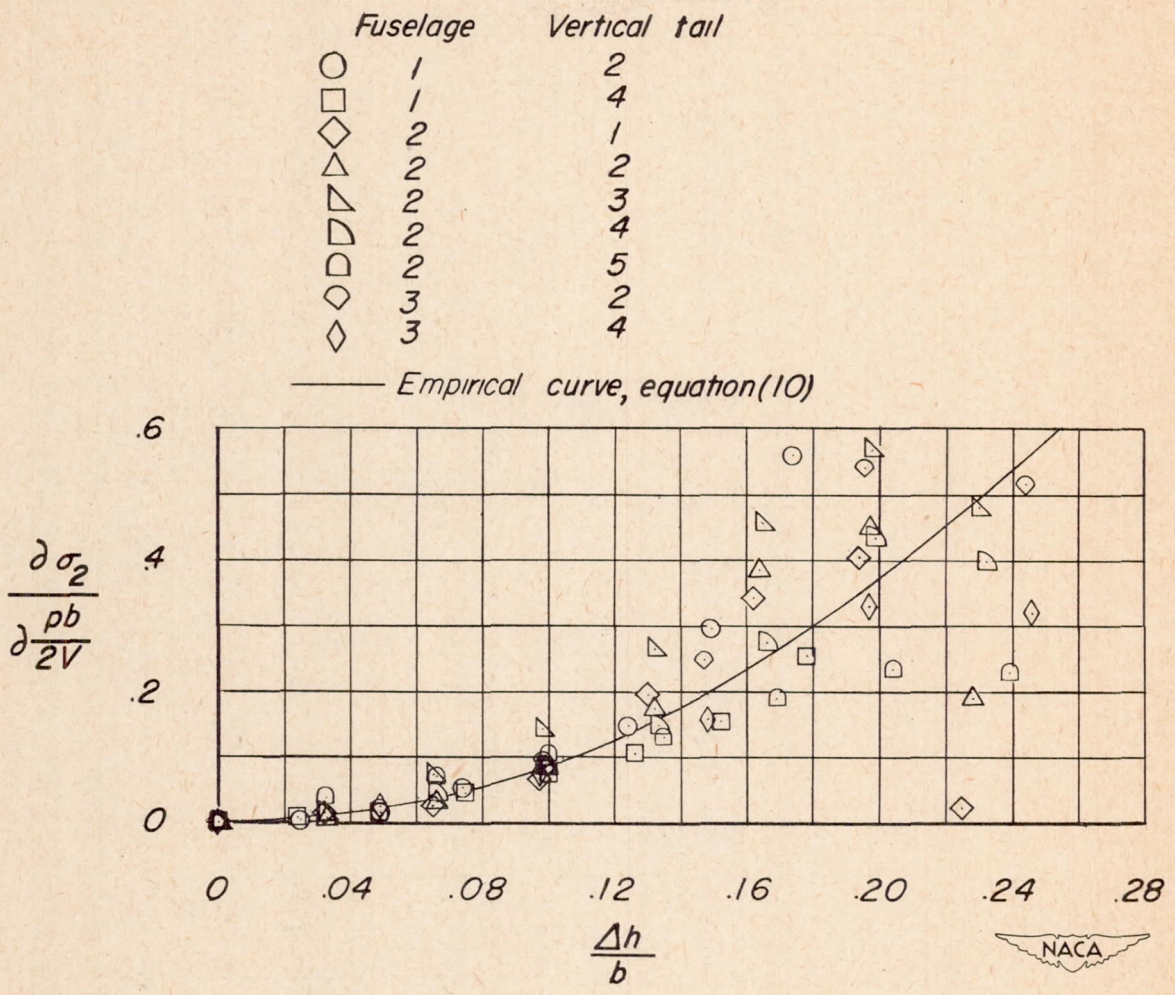
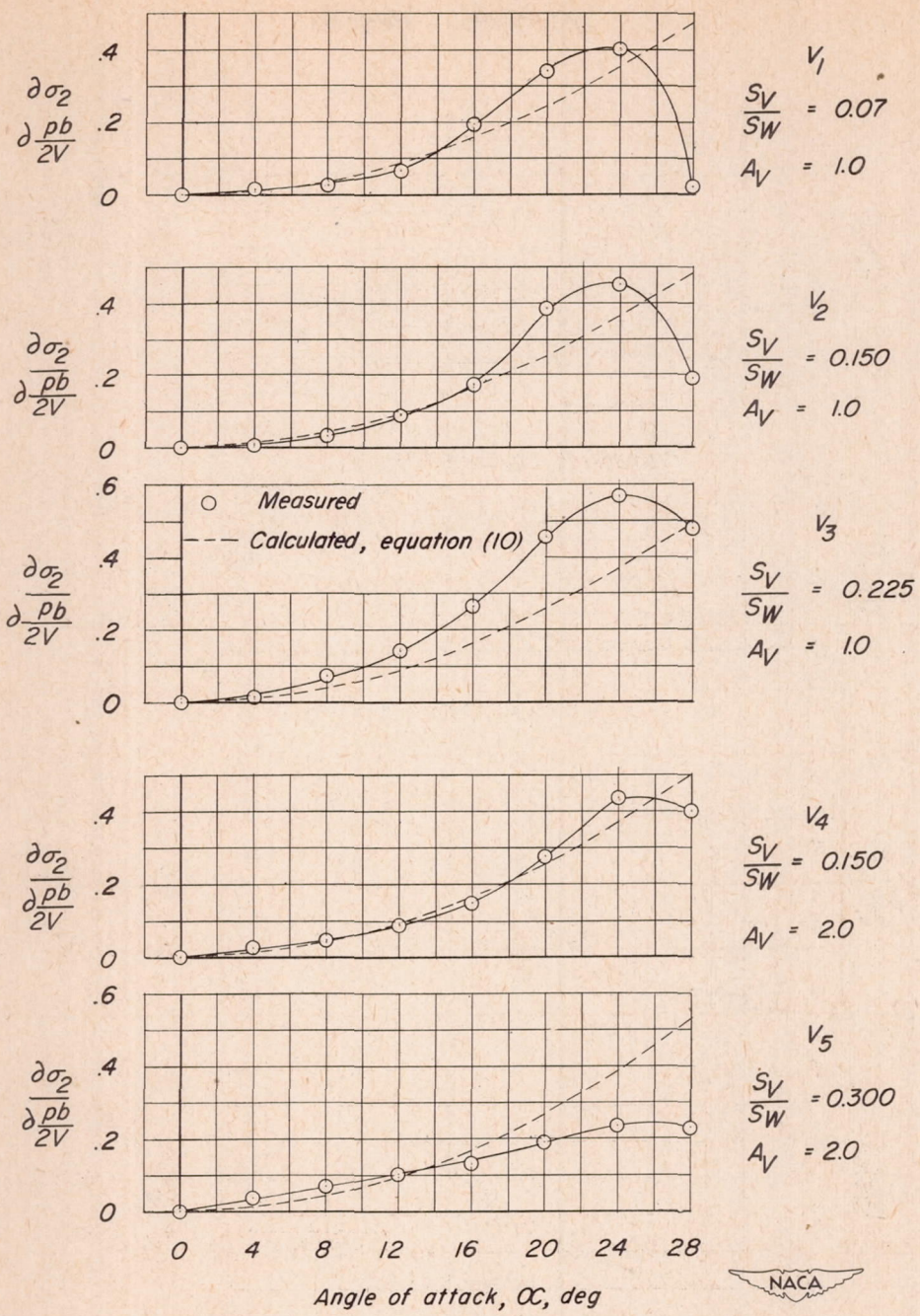
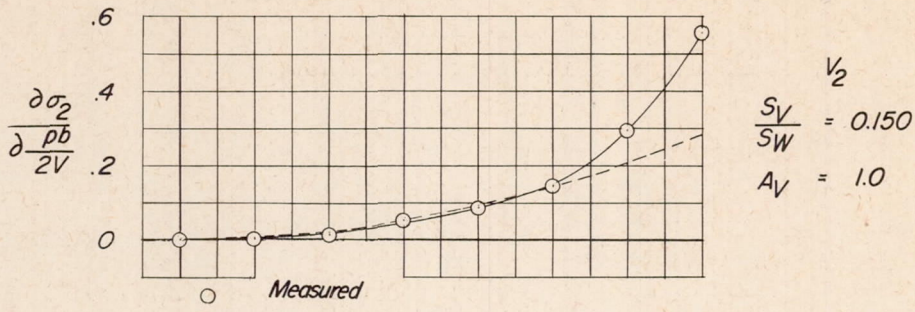


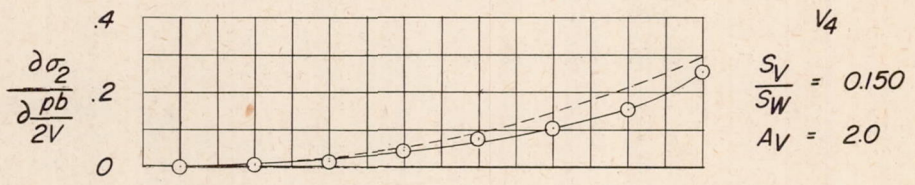
Figure 14.- Variation of $\frac{\partial \sigma_2}{\partial \frac{pb}{2V}}$ with $\Delta h/b$. Wing off.



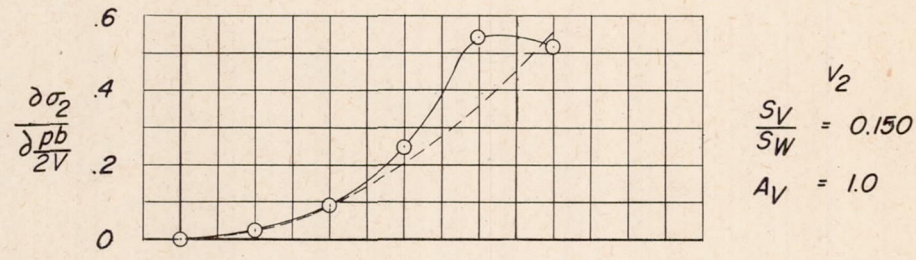
(a) Fuselage F_2.

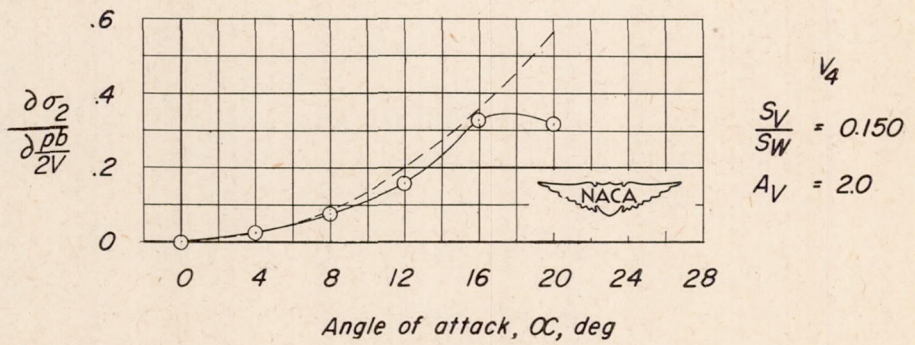
Figure 15.- Comparison of measured and calculated variation with angle of attack of $\frac{\partial \sigma_2}{\partial \frac{pb}{2V}}$. Wing off.





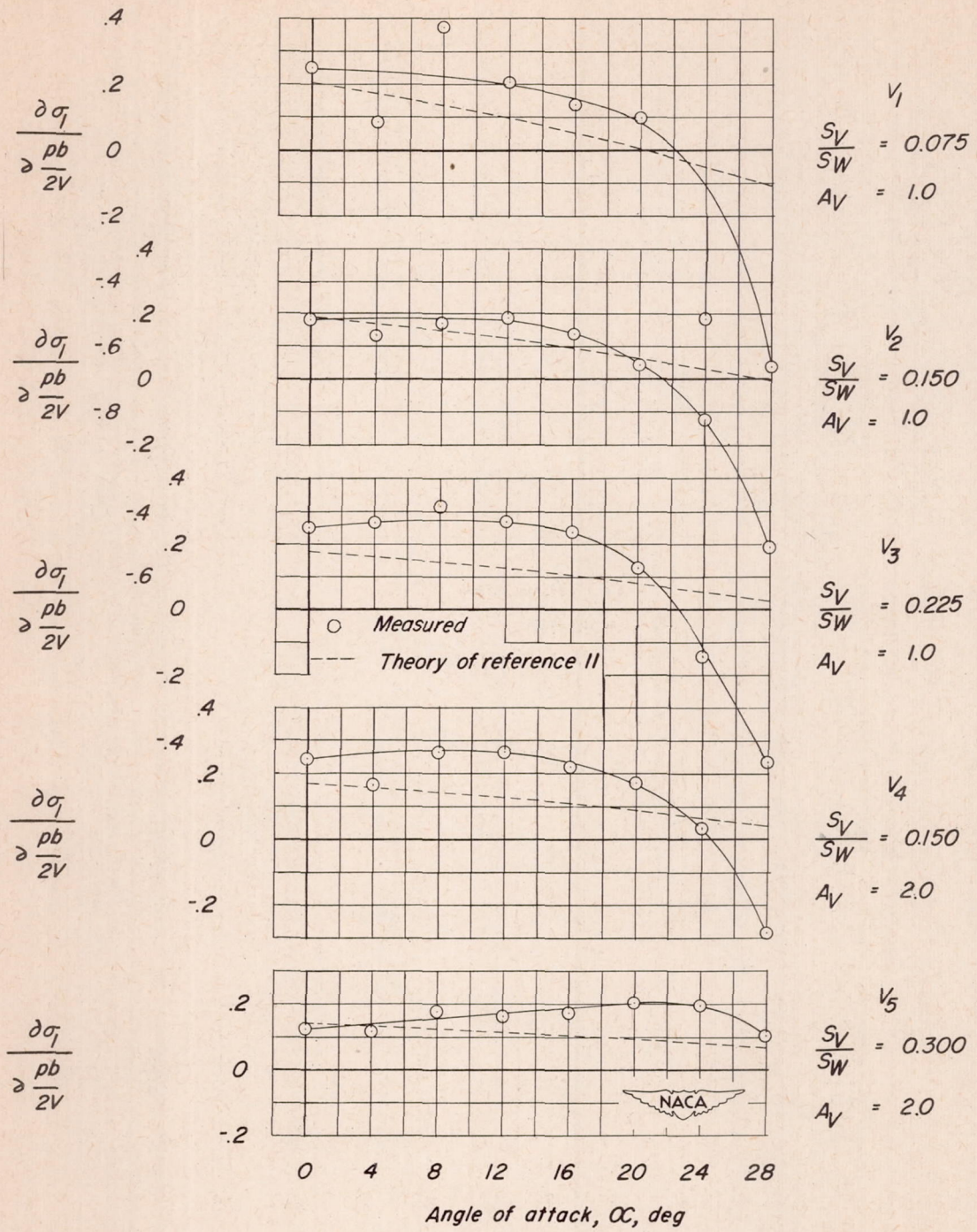
(b) Fuselage F_1.





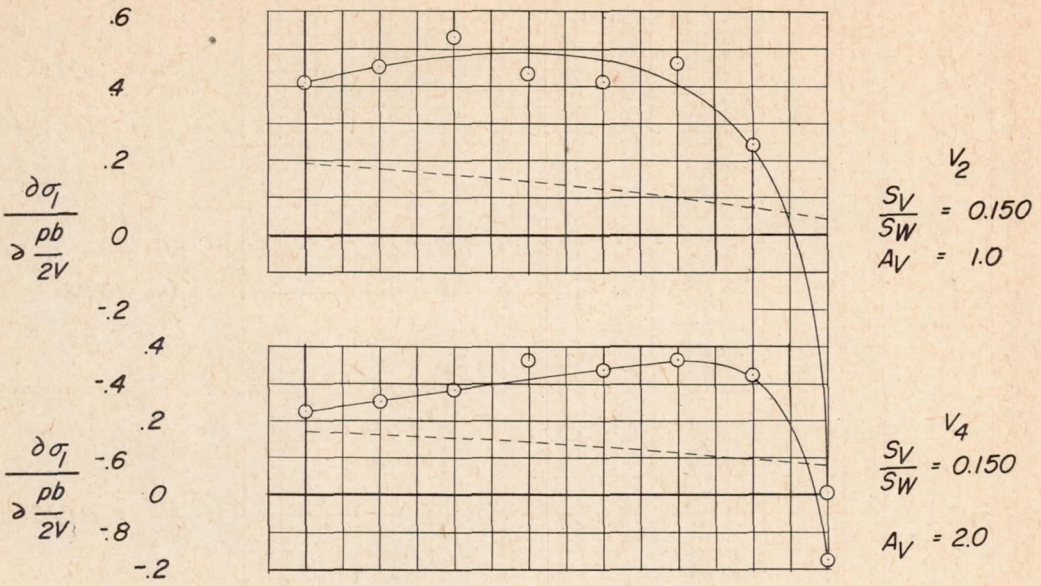
(c) Fuselage F_3.

Figure 15.- Concluded.



(a) Fuselage F_2.

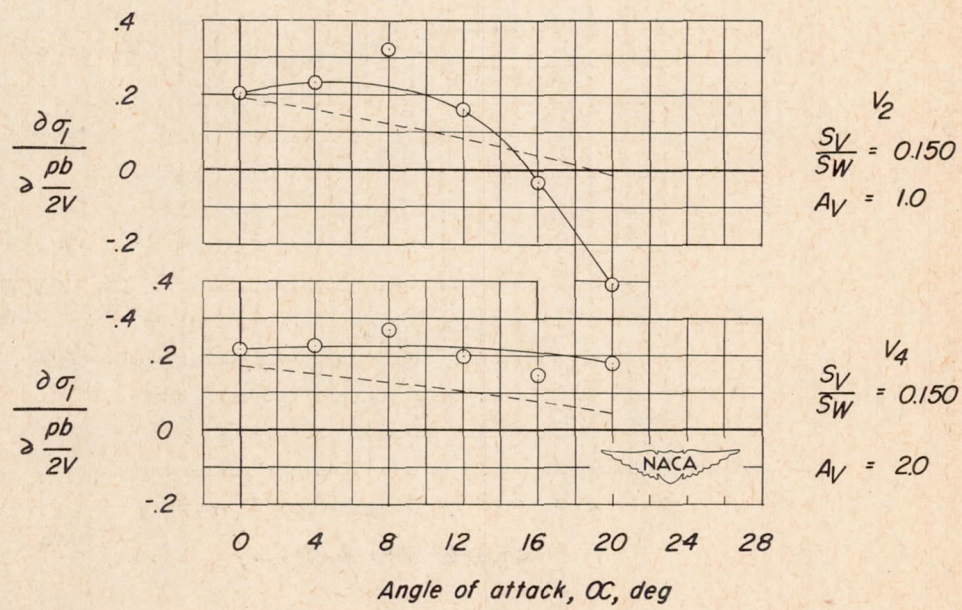
Figure 16.- Comparison of measured and calculated variation with angle of attack of $\frac{\partial \sigma_l}{\partial \frac{pb}{2V}}$.



(b) Fuselage F_1.

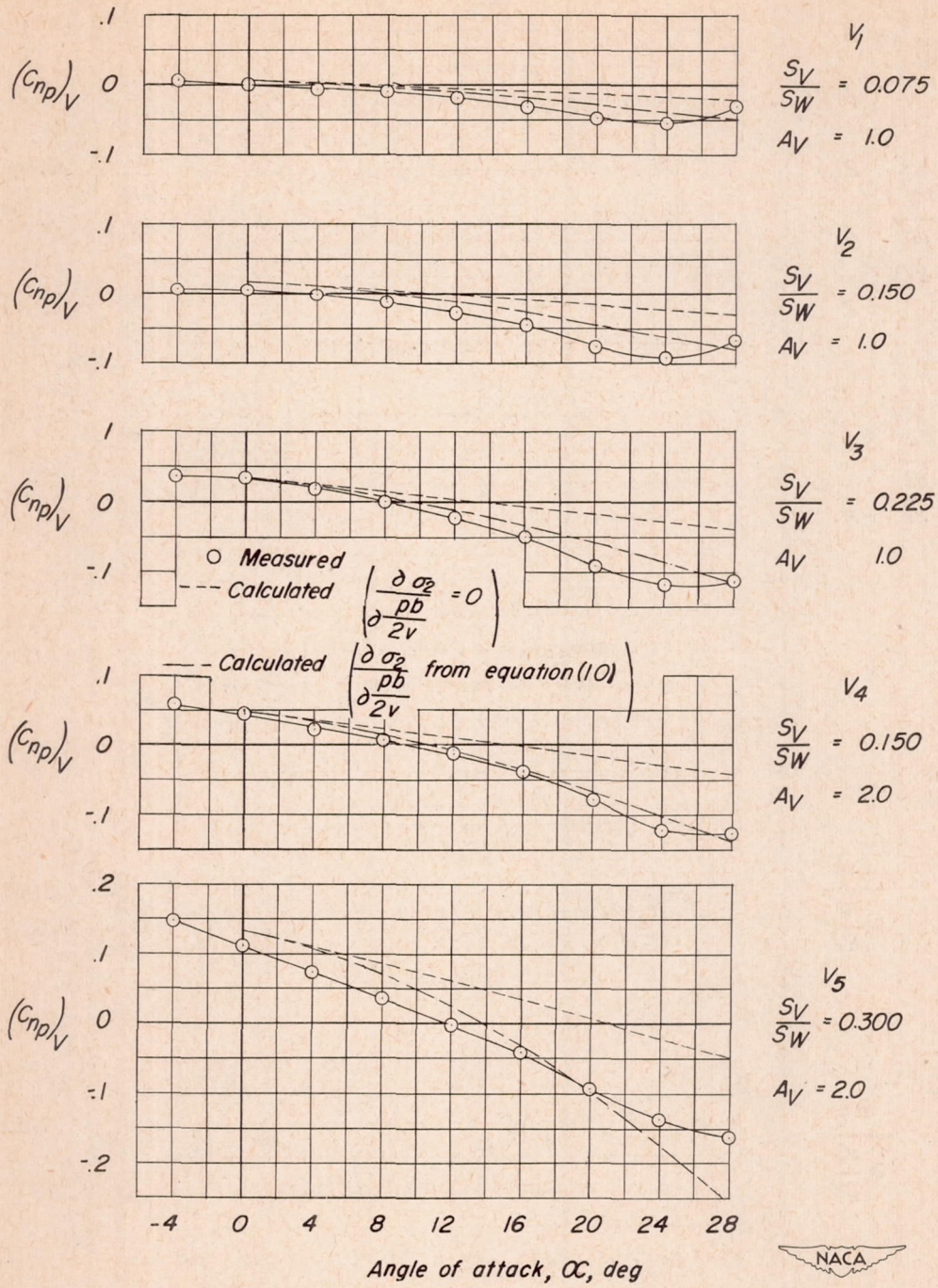
○ Measured

--- Theory of reference 11



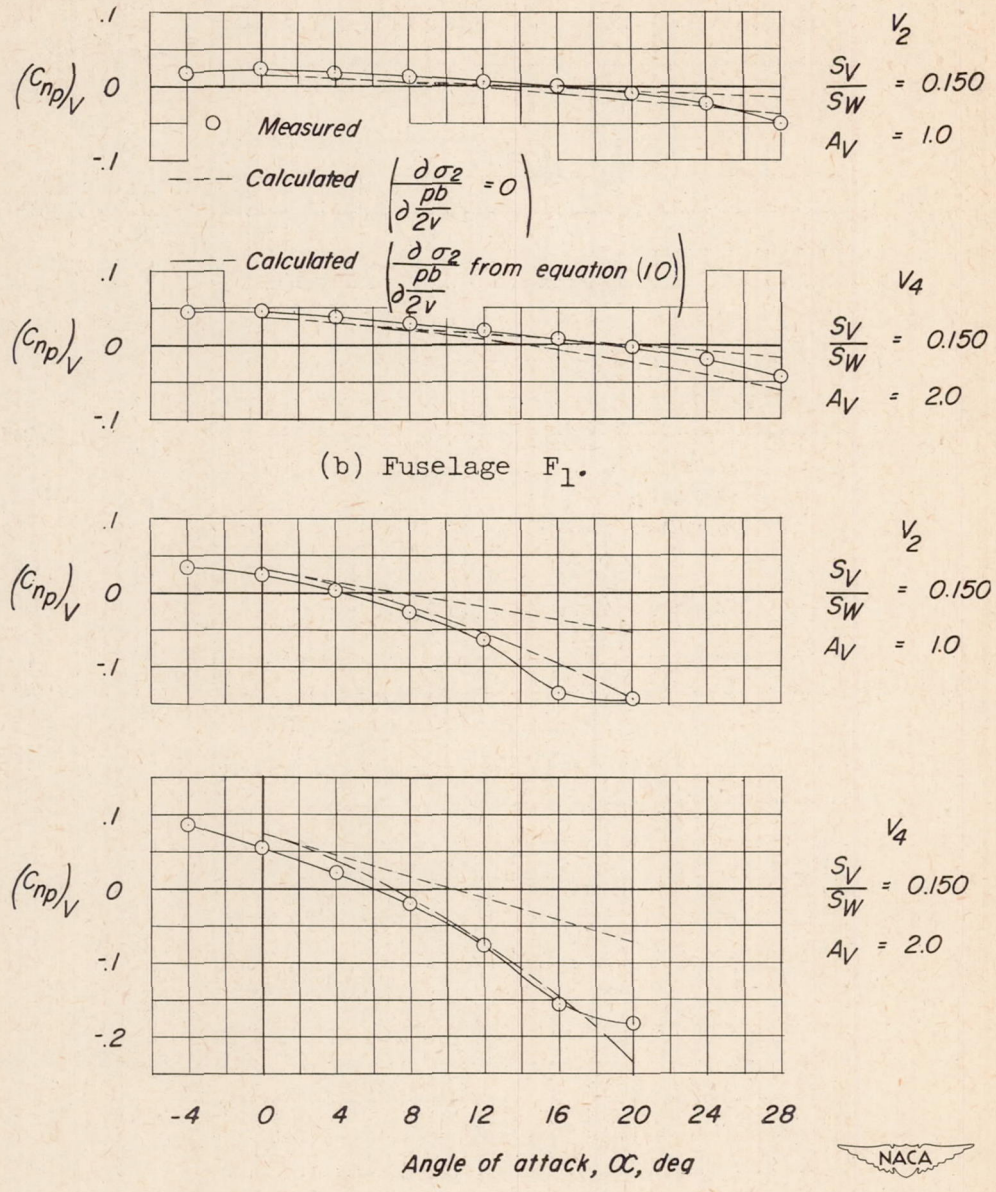
(c) Fuselage F_3.

Figure 16.- Concluded.



(a) Fuselage F_2.

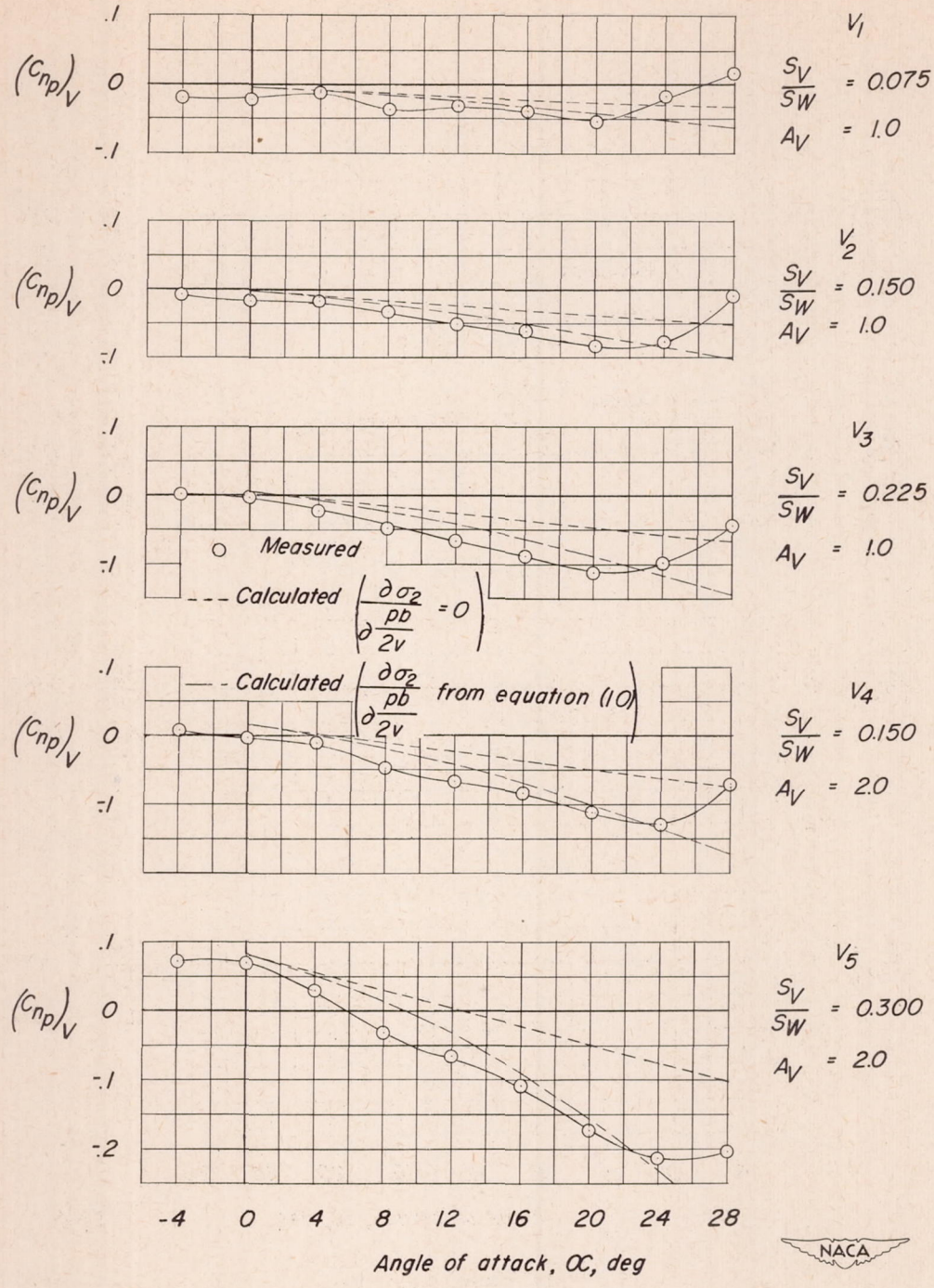
Figure 17.- Comparison of measured and calculated variation with angle of attack of $(C_{n_p})_V$. Wing off.



(b) Fuselage F_1.

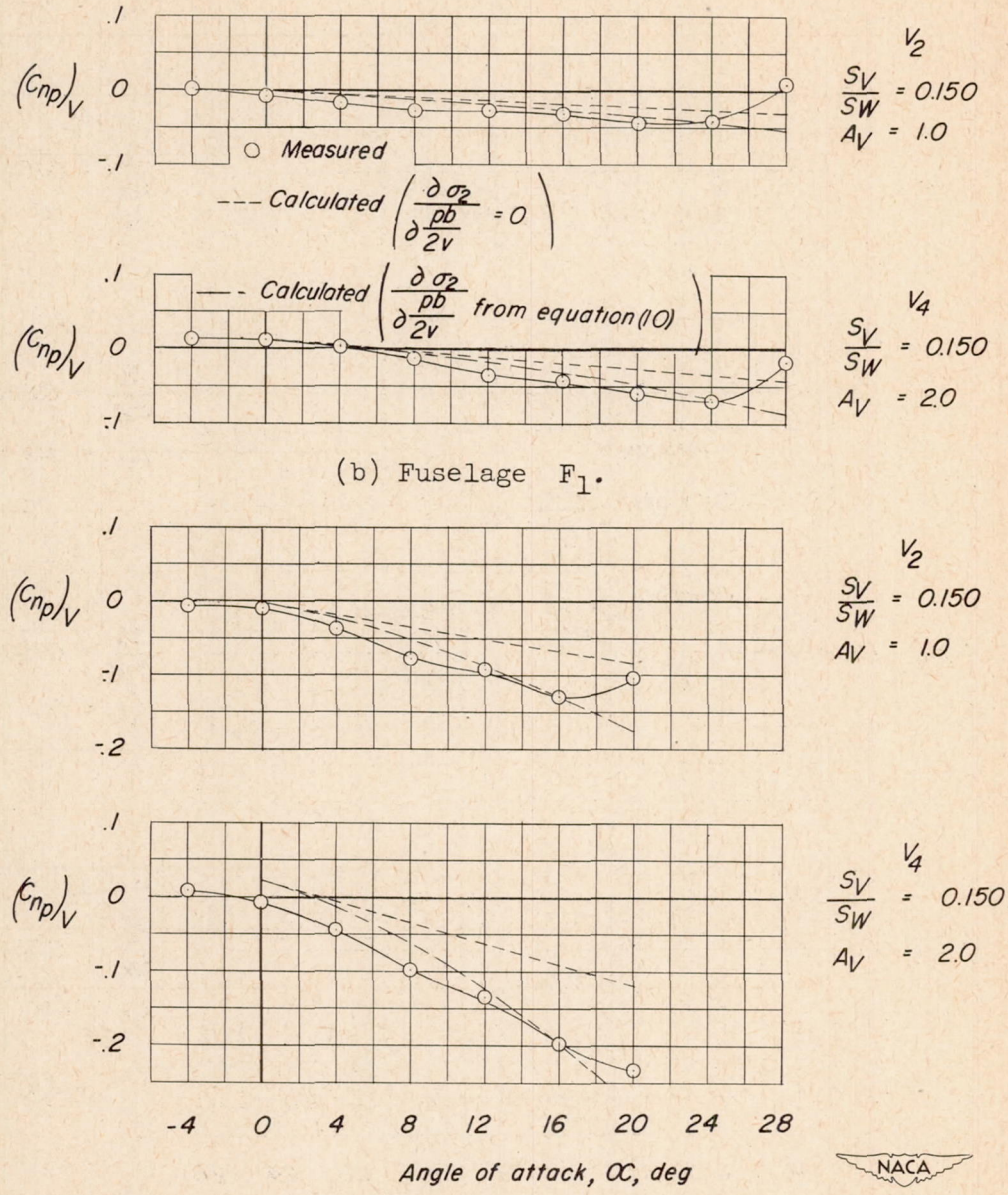
(c) Fuselage F_3.

Figure 17.- Concluded.



(a) Fuselage F_2.

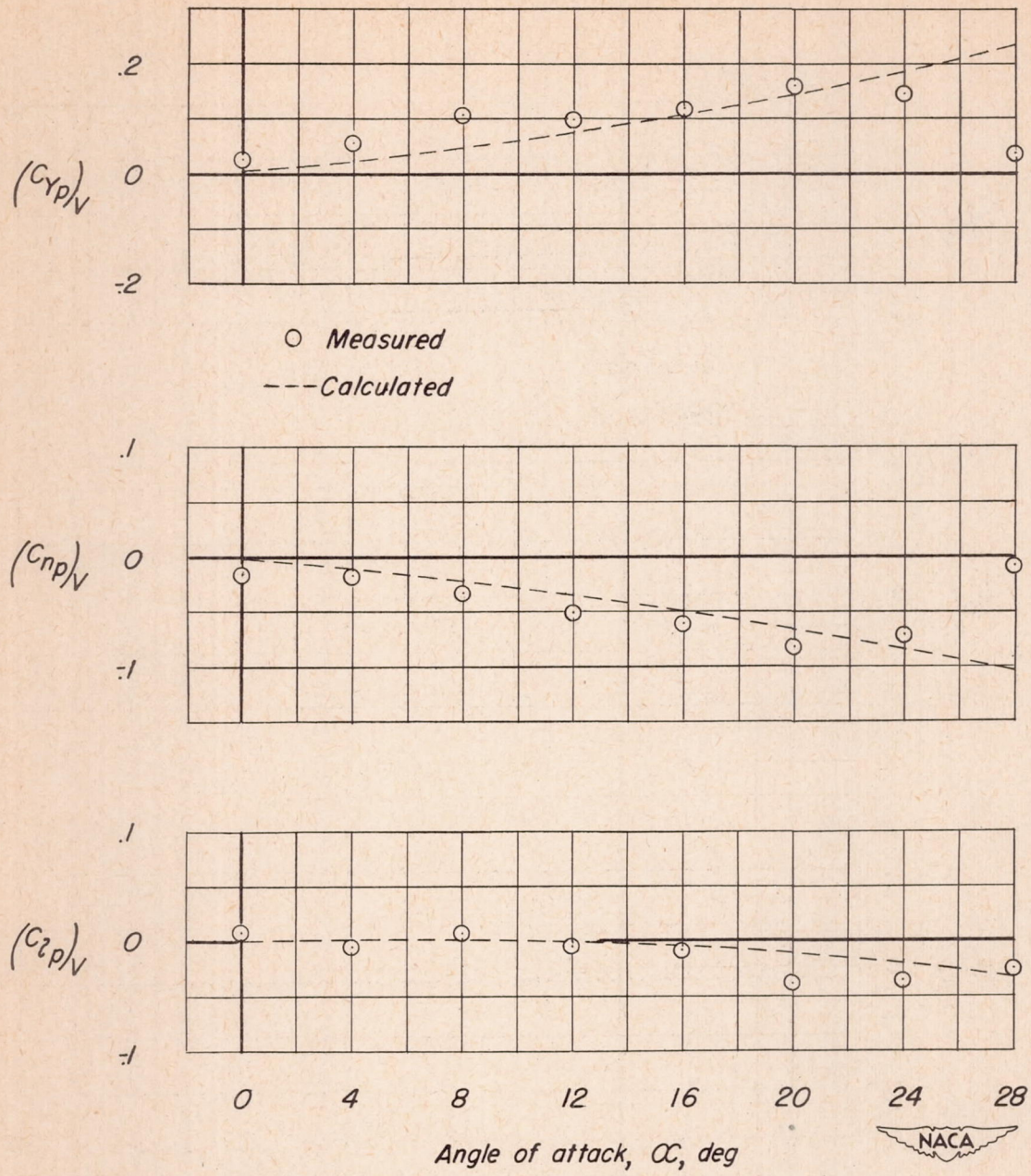
Figure 18.- Comparison of measured and calculated variation with angle of attack of $(C_{n_p})_V$. Wing on. Calculations based on $\frac{\partial \sigma_1}{\partial \frac{pb}{2V}}$ from reference 11.



(b) Fuselage F_1.

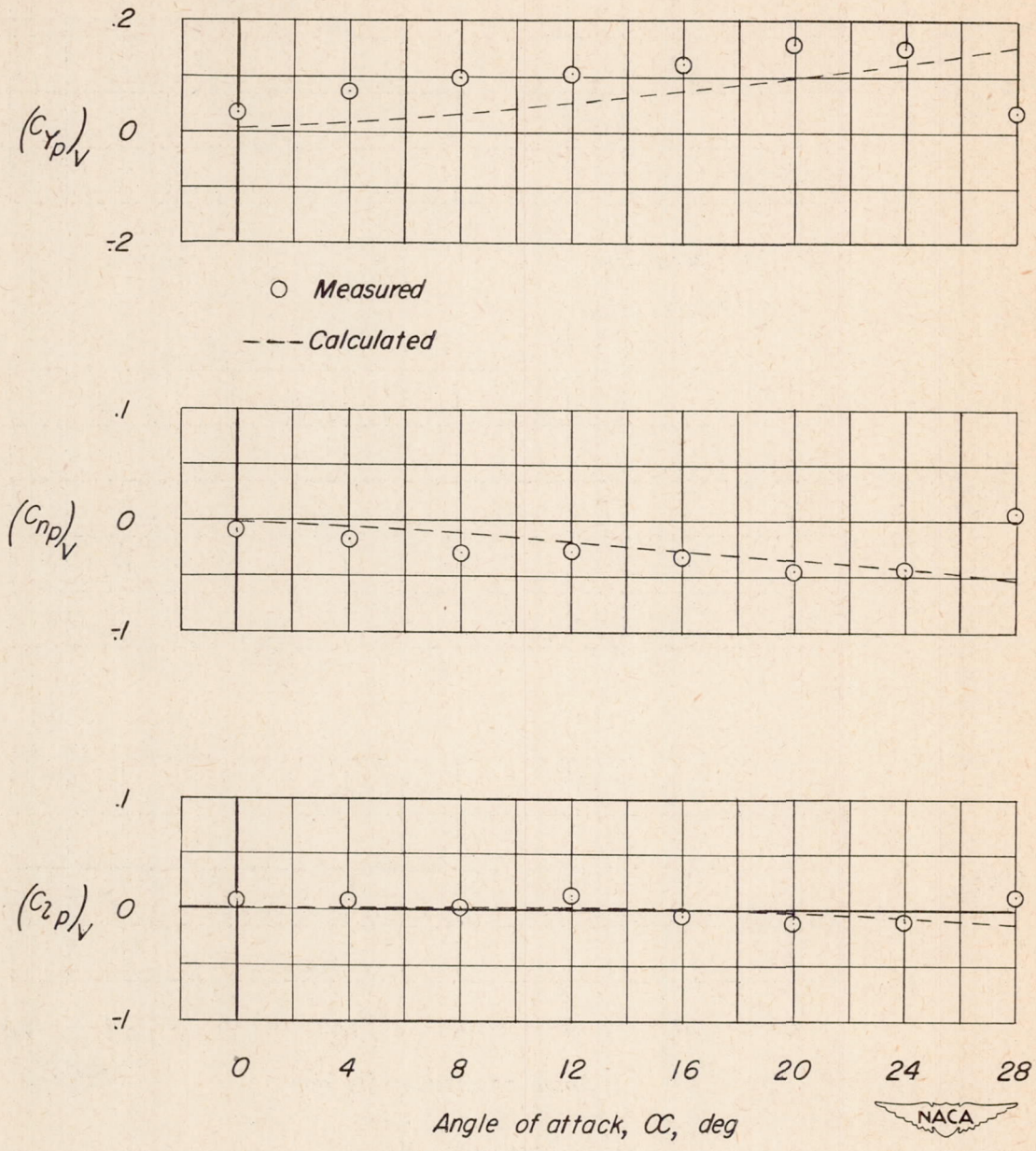
(c) Fuselage F_3.

Figure 18.- Concluded.



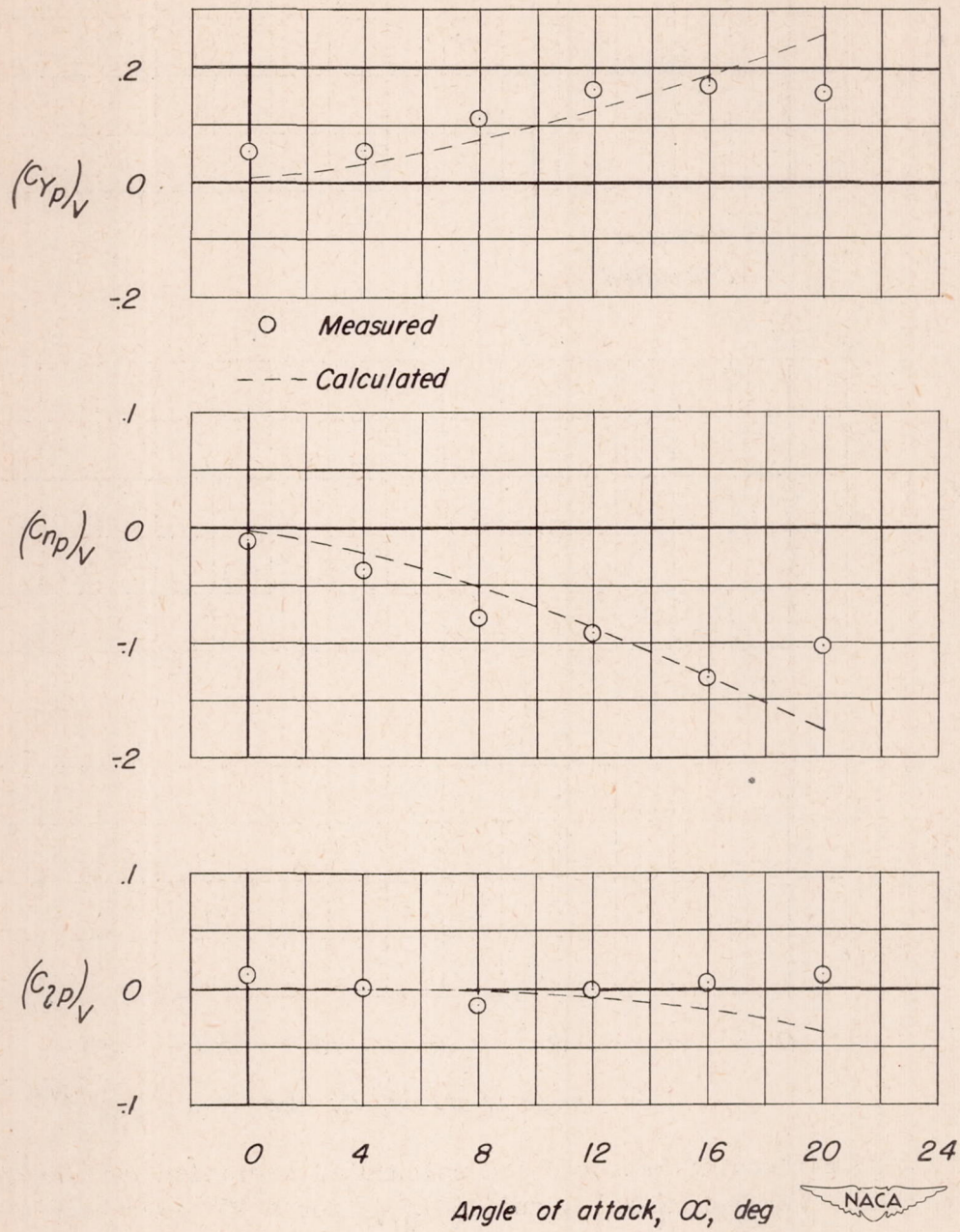
(a) Fuselage F_2.

Figure 19.- Comparison of measured and calculated variation with angle of attack of $\left(C_{Y_p}\right)_V$, $\left(C_{n_p}\right)_V$, and $\left(C_{l_p}\right)_V$ for the model with vertical tail V_2. Calculations based on $\left(\frac{\partial \sigma_1}{\partial \frac{pb}{2V}}\right)_{\alpha=0^\circ}$ from reference 11 and $\frac{\partial \sigma_2}{\partial \frac{pb}{2V}}$ from equation (10).



(b) Fuselage F_1.

Figure 19.- Continued.



(c) Fuselage F_3.

Figure 19.- Concluded.

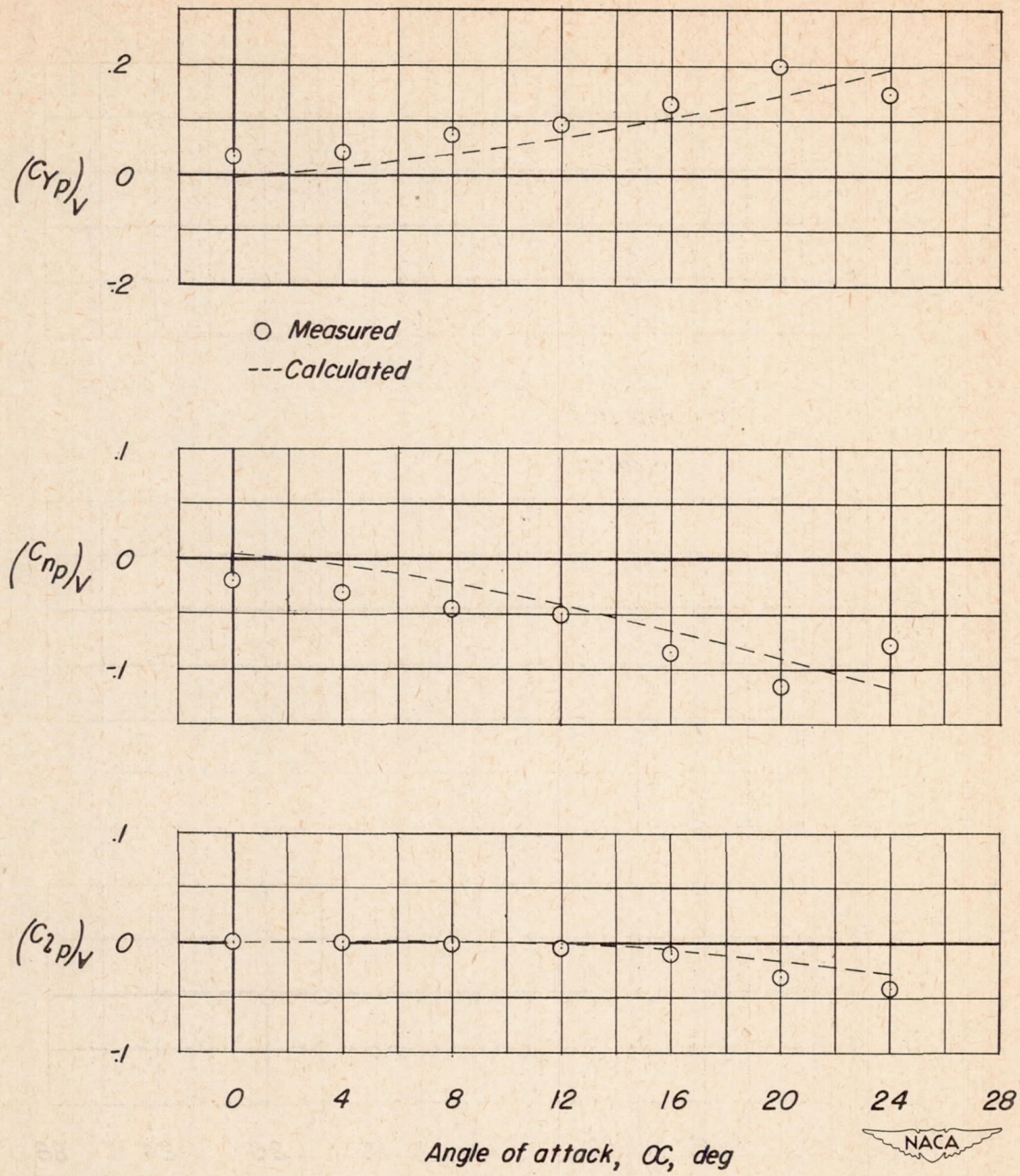


Figure 20.- Comparison of measured and calculated variation with angle of attack of $(C_{Y_p})_V$, $(C_{n_p})_V$, and $(C_{l_p})_V$ for a 45° sweptback midwing model (reference 12). Calculations based on $\left(\frac{\partial \sigma_1}{\partial \frac{pb}{2V}}\right)_{\alpha=0^\circ}$ from reference 11 and $\frac{\partial \sigma_2}{\partial \frac{pb}{2V}}$ from equation (10).

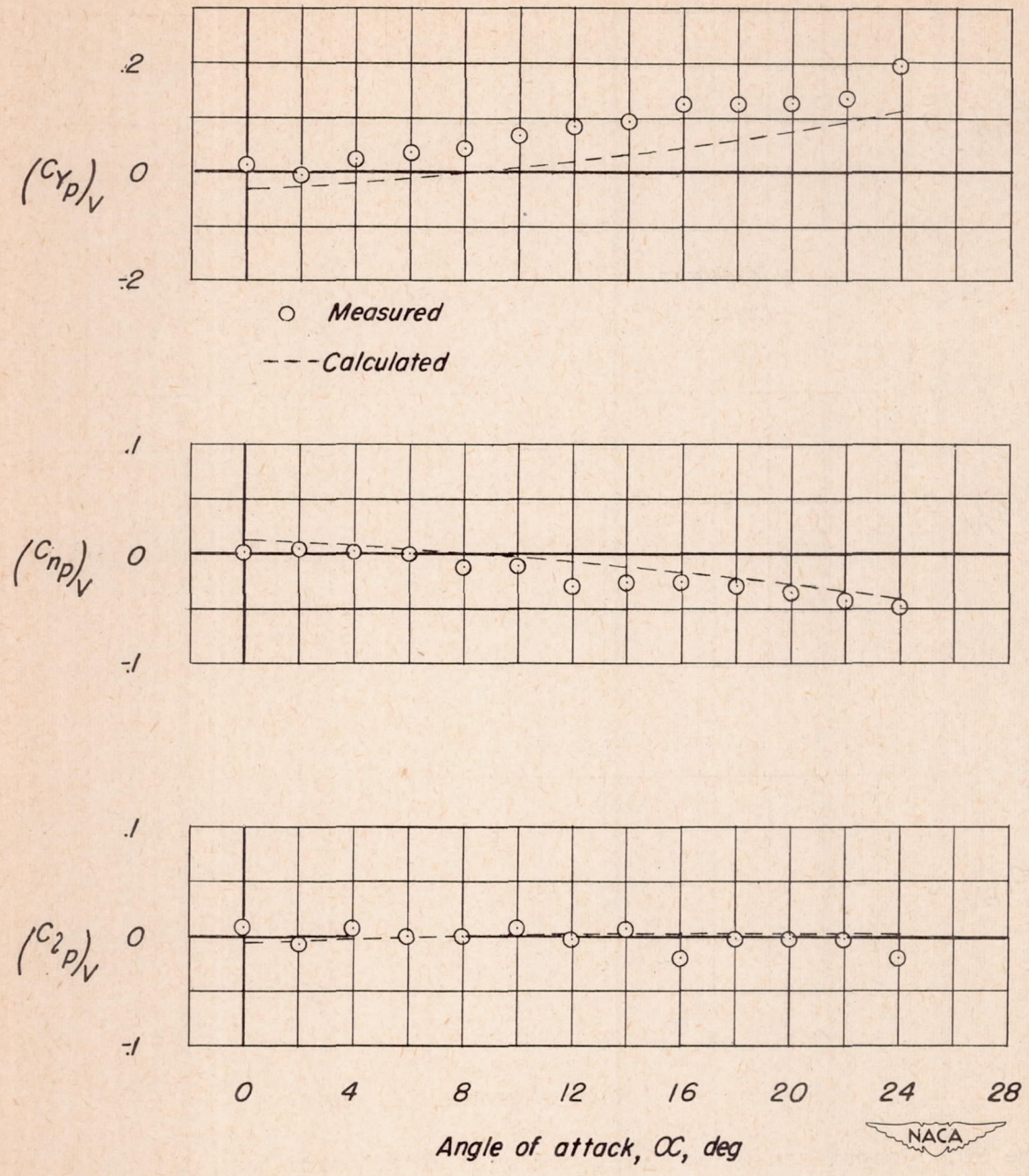


Figure 21.- Comparison of measured and calculated variation with angle of attack of $(C_{Y_p})_V$, $(C_{n_p})_V$, and $(C_{l_p})_V$ for a 41.57° sweptback near-midwing semitailless model (unpublished). Calculations based on $\left(\frac{\partial\sigma_1}{\partial\frac{pb}{2V}}\right)_{\alpha=0^\circ}$ from reference 11 and $\frac{\partial\sigma_2}{\partial\frac{pb}{2V}}$ from equation (10).

NACA-Langley - 12-26-51 - 1000